

Learn Goal-Conditioned Policy with Intrinsic Motivation for Deep Reinforcement Learning

Jinxin Liu¹²³ Donglin Wang^{23*} Qiangxing Tian¹²³ Zhengyu Chen¹²³

¹Zhejiang University. ²Westlake University. ³Westlake Institute for Advanced Study.
{liujinxin, wangdonglin, tianqiangxing, chenzhengyu}@westlake.edu.cn

Abstract

It is of significance for an agent to autonomously explore the environment and learn a widely applicable and general-purpose goal-conditioned policy that can achieve diverse goals including images and text descriptions. Considering such perceptually-specific goals, one natural approach is to reward the agent with a prior non-parametric distance over the embedding spaces of states and goals. However, this may be infeasible in some situations, either because it is unclear how to choose suitable measurement, or because embedding (heterogeneous) goals and states is non-trivial. The key insight of this work is that we introduce a latent-conditioned policy to provide goals and intrinsic rewards for learning the goal-conditioned policy. As opposed to directly scoring current states with regards to goals, we obtain rewards by scoring current states with associated latent variables. We theoretically characterize the connection between our unsupervised objective and the multi-goal setting, and empirically demonstrate the effectiveness of our proposed method which substantially outperforms prior techniques in a variety of tasks.

1 Introduction

Deep reinforcement learning (RL) makes it possible to drive agents to achieve sophisticated goals in complex and uncertain environments, from computer games (Badia et al. 2020; Berner et al. 2019) to real robot control (Lee et al. 2018; Lowrey et al. 2019; Vecerik et al. 2019; Popov et al. 2017), which usually involves learning a specific policy for individual task relying on hand-specifying reward function. However, autonomous agents are expected to exist persistently in the world and have the ability to reach diverse goals. To achieve this, one needs to design a mechanism to spontaneously generate diverse goals and the associated rewards, over which the goal-conditioned policy is trained.

Based on the space of goal manifold, previous works can be divided into two categories: *perceptually-specific goal based approaches* and *latent variable based methods*. In the former, previous approaches normally assume the spaces of perceptual goals and states are same, and sample goals from the historical trajectories of the policy to be trained. It is convenient to use a prior non-parametric measure function, such as L2 norm, to provide rewards (current states vs.

goals) over the state space or the embedding space (Higgins et al. 2017; Nair et al. 2018; Sermanet et al. 2018; Warde-Farley et al. 2019). However, these approaches taking the prior non-parametric measure function may limit the repertoires of behaviors and impose manual engineering burdens.

On the contrary, *latent variable based methods* assume that goals (latent variables) and states come from different spaces and the distribution of goals (latent variables) is known a priori. In parallel, such methods autonomously learn a reward function and a latent-conditioned policy through the lens of empowerment (Salge, Glackin, and Polani 2014; Eysenbach et al. 2018; Sharma et al. 2020). However, such policy is conditioned on latent variables rather than perceptually-specific goals. Applying this procedure to goal-reaching tasks, similar to the parameter initialization or hierarchical RL, needs an external reward function for new tasks; otherwise the learned latent-conditioned policy cannot be applied directly to perceptually-specific goals.

In this paper, we incorporate a latent variable based objective into the perceptual goal-reaching tasks. Specifically, we decouple the task generation (including perceptual goals and associated reward functions) and goal-conditioned policy optimization, which are often intertwined in prior approaches. For the task generation, we employ a latent variable based objective (Eysenbach et al. 2018) to learn a latent-conditioned policy, run to generate goals, and a discriminator, serve as the reward function. Then our goal-conditioned policy is rewarded by the discriminator to imitate the trajectories, relabeled as goals, induced by the latent-conditioned policy. This procedure enables the acquired discriminator as a proxy to reward the goal-conditioned policy for various relabeled goals. *In essence, the latent-conditioned policy can reproducibly influence the environment, and the goal-conditioned policy perceptibly imitates these influences.*

The main contribution of our work is an unsupervised RL method that can learn a perceptual goal-conditioned policy via intrinsic motivation (GPIM). Our training procedure decouples the task (goals and rewards) generation and policy optimization, which makes the obtained reward function universal and effective for various relabeled goals, including images and texts. We formally analyze the effectiveness of our relabeling procedure, and empirically find that our intrinsic reward is well shaped by the environment’s dynamics and as a result benefits the training efficiency on extensive tasks.

*Corresponding author.

2 Preliminaries

The goal in a reinforcement learning problem is to maximize the expected return in a Markov decision process (MDP) \mathcal{M} , defined by the tuple (S, A, p, r, γ) , where S and A are state and action spaces, $p(s_{t+1}|s_t, a_t)$ gives the next-state distribution upon taking action a_t in state s_t , $r(s_t, a_t, s_{t+1})$ is the reward received at transition $s_t \xrightarrow{a_t} s_{t+1}$, and γ is a discount factor. The objective is to learn the policy $\pi_\theta(a_t|s_t)$ by maximizing $\mathbb{E}_{p(\tau; \theta)} [R(\tau)] = \mathbb{E}_{p(\tau; \theta)} [\sum_t \gamma^t r(s_t, a_t, s_{t+1})]$, where $p(\tau; \theta)$ denotes the induced trajectories by policy π_θ in the environment: $p(\tau; \theta) = p(s_0) \cdot \prod_{t=0}^{T-1} \pi_\theta(a_t|s_t) p(s_{t+1}|s_t, a_t)$.

Multi-goal RL augments the above optimization with a goal g by learning a goal-conditioned policy $\pi_\theta(a_t|s_t, g)$ and optimizing $\mathbb{E}_{p(g)} \mathbb{E}_{p(\tau|g; \theta)} [R(\tau)]$ with reward $r(s_t, a_t, s_{t+1}, g)$. Such optimization can also be interpreted as a form of mutual information between the goal g and agent’s trajectory τ (Warde-Farley et al. 2019):

$$\max \mathcal{I}(\tau; g) = \mathbb{E}_{p(g)p(\tau|g; \theta)} [\log p(g|\tau) - \log p(g)]. \quad (1)$$

If $\log p(g|\tau)$ is unknown and the goal g is a latent variable, latent variable based models normally maximize the mutual information between the latent variable ω and agent’s behavior b , and lower-bound this mutual information by approximating the posterior $p(\omega|b)$ with a learned $q_\phi(\omega|b)$: $\mathcal{I}(b; \omega) \geq \mathbb{E}_{p(\omega, b; \mu)} [\log q_\phi(\omega|b) - \log p(\omega)]$, where the specific manifestation of agent’s behavior b can be an entire trajectory τ , an individual state s or a final state s_T . It is thus applicable to train $\pi_\mu(a_t|s_t, \omega)$ with learned q_ϕ (as reward).

Several prior works have sought to incorporate the latent-conditioned $\pi_\mu(a_t|s_t, \omega)$ (as low-level skills) into hierarchical RL (Zhang, Yu, and Xu 2021) or reuse the learned q_ϕ (as predefined tasks) in meta-RL (Gupta et al. 2018), while we claim to reuse *both* π_μ and q_ϕ with our relabeling procedure.

3 The Method

In this section, we first formalize the problem and introduce the framework. Second, we illustrate our GPIM objective and elaborate on the process of how to jointly learn the latent-conditioned policy and a goal-conditioned policy. Third, we formally verify our (unsupervised) objective and understand how GPIM relates to the standard multi-goal RL.

3.1 Overview

As shown in Figure 1 (right), our objective is to learn a goal-conditioned policy $\pi_\theta(a|\tilde{s}, g)$ that inputs state \tilde{s} and perceptually-specific goal g and outputs action a . To efficiently generate tasks for training the goal-conditioned policy π_θ , we introduce another latent-conditioned policy $\pi_\mu(a|s, \omega)$, which takes as input a state s and a latent variable ω and outputs action a to generate goals, and the associated discriminator q_ϕ (i.e., generating tasks). Additionally, we assume that we have access to a procedural relabeling function f_κ (we will discuss this assumption latter), which can relabel states s as goals g for training π_θ . On this basis, $\pi_\theta(a|\tilde{s}, g)$ conditioned on the relabeled goal g interacts with the reset environment under the instruction of the associated

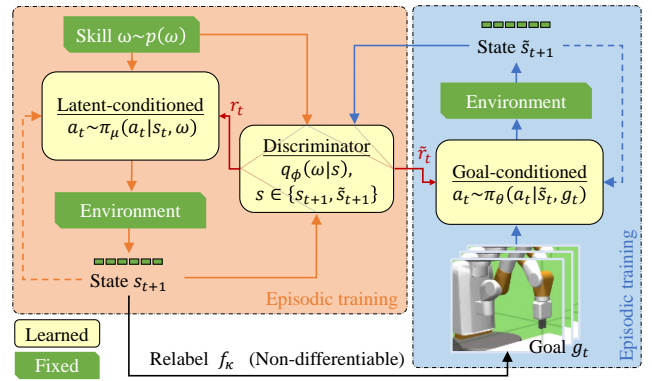


Figure 1: Framework of GPIM. We jointly train the latent-conditioned policy π_μ and the discriminator q_ϕ to understand skills which specify task objectives (e.g., trajectories, the final goal state), and use such understanding to reward the goal-conditioned policy π_θ for completing such tasks (relabelled states). In this diagram, state s_{t+1} (e.g., joints) induced by π_μ is converted into the perceptually-specific goal g_t (e.g., images or text descriptions) for π_θ . Note that the two environments above are same, and the initial states s_0 of π_μ and \tilde{s}_0 of π_θ are sampled from the same (fixed) distribution.

q_ϕ . We use the non-tilde s and the tilde \tilde{s} to distinguish between the states of two policies respectively. Actually, \tilde{s} and s come from the same state space. In the following, if not specified, goal g refers to the perceptually-specific goal, and no longer includes the case that goal is a latent variable.

To ensure the generated tasks (by π_μ) are reachable for π_θ , we explicitly make the following assumption¹:

Assumption 1 *The initial state of the environment is fixed.*

3.2 Proposed GPIM Method

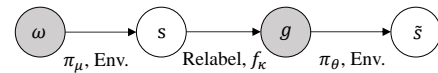


Figure 2: Latent-conditioned policy π_μ provides goals and the associated reward for the goal-conditioned policy π_θ .

In order to jointly learn the latent-conditioned $\pi_\mu(a|s, \omega)$ and goal-conditioned $\pi_\theta(a|\tilde{s}, g)$, we maximize the mutual information between the state s and latent variable ω for π_μ , and simultaneously maximize the mutual information between the state \tilde{s} and goal g for π_θ . Consequently, the overall objective to be maximized can be expressed as follows²

$$\mathcal{F}(\mu, \theta) = \mathcal{I}(s; \omega) + \mathcal{I}(\tilde{s}; g). \quad (2)$$

For clarification, Figure 2 depicts the graphical model for the latent variable ω , state s induced by π_μ , goal g relabeled

¹In appendix, we empirically find the assumption can be lifted.

²To further clarify the motivation, we conduct the ablation study to compare our method (maximizing $\mathcal{I}(s; \omega) + \mathcal{I}(\tilde{s}; g)$) with that just maximizing $\mathcal{I}(\tilde{s}; \omega)$ and that maximizing $\mathcal{I}(\tilde{s}; g)$ in appendix.

from s , and state \tilde{s} induced by π_θ . As seen, the latent variable $\omega \sim p(\omega)$ is firstly used to generate state s via the policy π_μ interacting with the environment. Then, we relabel the generated state s to goal g . After that, π_θ conditioned on g interacts with the environment to obtain the state \tilde{s} at another episode. In particular, π_μ is expected to generate diverse behavior modes by maximizing $\mathcal{I}(s; \omega)$, while π_θ behaving like \tilde{s} is to "imitate" (see next q_ϕ) these behaviors by taking as input the relabeled goal (indicated by Figure 2).

Based on the context, the correlation between \tilde{s} and g is no less than that between \tilde{s} and ω : $\mathcal{I}(\tilde{s}; g) \geq \mathcal{I}(\tilde{s}; \omega)$ (Beaudry and Renner 2011). Thus, we can obtain the lower bound:

$$\begin{aligned} \mathcal{F}(\mu, \theta) &\geq \mathcal{I}(s; \omega) + \mathcal{I}(\tilde{s}; \omega) \\ &= 2\mathcal{H}(\omega) + \mathbb{E}_{p_m(\cdot)} [\log p(\omega|s) + \log p(\omega|\tilde{s})], \end{aligned} \quad (3)$$

where $p_m(\cdot) \triangleq p(\omega, s, g, \tilde{s}; \mu, \kappa, \theta)$ denotes the joint distribution of ω, s, g and \tilde{s} specified by the graphic model in Figure 2. Since it is difficult to exactly compute the posterior distributions $p(\omega|s)$ and $p(\omega|\tilde{s})$, Jensen's Inequality (Barber and Agakov 2003) is further applied for approximation by using a learned discriminator network $q_\phi(\omega|\cdot)$. Thus, we have $\mathcal{F}(\mu, \theta) \geq \mathcal{J}(\mu, \phi, \theta)$, where

$$\mathcal{J}(\mu, \phi, \theta) \triangleq 2\mathcal{H}(\omega) + \mathbb{E}_{p_m(\cdot)} [\log q_\phi(\omega|s) + \log q_\phi(\omega|\tilde{s})].$$

It is worth noting that the identical discriminator q_ϕ is used for the variational approximation of $p(\omega|s)$ and $p(\omega|\tilde{s})$. For the state s induced by skill $\pi_\mu(\cdot|\cdot, \omega)$ and \tilde{s} originating from $\pi_\theta(\cdot|\cdot, g)$, the shared discriminator q_ϕ assigns a similarly high probability on ω for both states s and \tilde{s} associated with the same ω . Therefore, q_ϕ can be regarded as a reward network shared by the latent-conditioned π_μ and goal-conditioned π_θ . Intuitively, we factorize acquiring the goal-conditioned policy π_θ and learn it purely in the space of the agent's embodiment (i.e., the latent ω) — separate from the perceptually-specific goal g (e.g., states, images and texts), where the latent ω and the perceptual goal g have different characteristics due to the underlying manifold spaces.

According to the surrogate objective $\mathcal{J}(\mu, \phi, \theta)$, we propose an alternating optimization between π_μ, q_ϕ and π_θ :

Step I: Fix π_θ and update π_μ and q_ϕ . In this case, θ is not a variable to update and thus $\mathcal{J}(\mu, \phi, \theta)$ becomes

$$\begin{aligned} \mathcal{J}(\mu, \phi) &= \mathbb{E}_{p(\omega, s; \mu)} [\log q_\phi(\omega|s)] \\ &\quad + \underbrace{\mathbb{E}_{p_m(\cdot)} [\log q_\phi(\omega|\tilde{s}) - 2 \log p(\omega)]}_{\text{Variable independent term}}. \end{aligned} \quad (4)$$

According to Equation 4, π_μ can be thus optimized by setting the intrinsic reward at time step t as

$$r_t = \log q_\phi(\omega|s_{t+1}) - \log p(\omega), \quad (5)$$

where the term $-\log p(\omega)$ is added for agents to avoid artificial termination and reward-hacking issues (Amodei et al. 2016; Eysenbach et al. 2018). We implement this optimization with SAC. In parallel, the reward network (discriminator) q_ϕ can be updated with SGD by maximizing

$$\mathbb{E}_{p(\omega)p(s|\omega; \mu)} [\log q_\phi(\omega|s)]. \quad (6)$$

Algorithm 1: Learning process of our proposed GPIM

```

1: while not converged do
2:   # Step I: generate goals and reward functions.
3:   Sample the latent variable:  $\omega \sim p(\omega)$ .
4:   Reset Env. & sample initial state:  $s_0 \sim p_0(s)$ .
5:   for  $t = 0, 1, \dots, T - 1$  steps do
6:     Sample action:  $a_t \sim \pi_\mu(a_t|s_t, \omega)$ .
7:     Step environment:  $s_{t+1} \sim p(s_{t+1}|s_t, a_t)$ .
8:     Relabel:  $g_t = f_\kappa(s_{t+1})$ .  $\triangleright$  Record.
9:     Compute reward  $r_t$  for policy  $\pi_\mu$  using (5).
10:    Update policy  $\pi_\mu$  to maximize  $r_t$  with SAC.
11:    Update discriminator ( $q_\phi$ ) to maximize (6) with SGD.
12:  end for
13:  # Step II:  $\pi_\theta$  imitates  $\pi_\mu$  with the relabeled goals and the
    associated rewards (for the same  $\omega$ ).
14:  Reset Env. & sample initial state:  $\tilde{s}_0 \sim p_0(\tilde{s})$ .
15:  for  $t = 0, 1, \dots, T - 1$  steps do
16:    Recap dynamic (time-varying) goal  $g_t$  from the recorded
    goals in line 8. # Note:  $g_t = g_T$  for static (fixed) goals.
17:    Sample action:  $a_t \sim \pi_\theta(a_t|\tilde{s}_t, g_t)$ .
18:    Step environment:  $\tilde{s}_{t+1} \sim p(\tilde{s}_{t+1}|\tilde{s}_t, a_t)$ .
19:    Compute reward  $\tilde{r}_t$  for policy  $\pi_\theta$  using (8).
20:    Update policy  $\pi_\theta$  to maximize  $\tilde{r}_t$  with SAC.
21:  end for
22: end while

```

Step II: Fix π_μ and q_ϕ to update π_θ . In this case, μ and ϕ are not variables to update, and $\mathcal{J}(\mu, \phi, \theta)$ can be simplified as

$$\begin{aligned} \mathcal{J}(\theta) &= \mathbb{E}_{p_m(\cdot)} [\log q_\phi(\omega|\tilde{s})] \\ &\quad + \underbrace{\mathbb{E}_{p(\omega, s; \mu)} [\log q_\phi(\omega|s) - 2 \log p(\omega)]}_{\text{Variable independent term}}. \end{aligned} \quad (7)$$

According to Equation 7, π_θ can thus be optimized by setting the intrinsic reward at time step t as

$$\tilde{r}_t = \log q_\phi(\omega|\tilde{s}_{t+1}) - \log p(\omega), \quad (8)$$

where the term $-\log p(\omega)$ is added for the same reason as above and we also implement this optimization with SAC. Note that we do not update q_ϕ with the data induced by π_θ .

These two steps are performed alternately until convergence (see Algorithm 1). In summary, we train the goal-conditioned π_θ along with an extra latent-conditioned π_μ and a procedural relabel function f_κ , which explicitly decouples the procedure of unsupervised RL into task generation (including goals and reward functions) and policy optimization.

For clarity, we state three different settings for f_κ : (1) if $f_\kappa = q_\phi$, our objective is identical to the latent variable based models, maximizing $\mathcal{I}(\omega; s)$ to obtain the *latent-conditioned* policy (Eysenbach et al. 2018); (2) if $f_\kappa(s) = s$, this procedure is consistent with the hindsight relabeling (Andrychowicz et al. 2017); (3) if $f_\kappa(s)$ and s have different spaces (not latent spaces), this relabeling is also a reasonable belief under the semi-supervised setting, e.g., the social partner in Colas et al. (2020). In our experiment, we will consider (2) and (3) to learn $\pi_\theta(\cdot|\cdot, g)$ that is conditioned *perceptually-specific* goals. For (3), it is easy to procedurally generate the image-based goals from (joint-based) states with the MuJoCo Physics Engine's (Todorov, Erez, and Tassa 2012) built-in renderer. Facing high-dimensional

goals, we also incorporate a self-supervised loss over the perception-level (Hafner et al. 2020; Lu et al. 2020) for π_θ .

3.3 Theoretical Analysis

Normally, multi-goal RL seeks the goal-conditioned policy $\pi_\theta(a|\tilde{s}, g)$ that maximizes $\mathcal{I}(\tilde{s}; g)$ with prior goal-distribution $p'(g)$ and the associated reward $p'(g|\tilde{s})$, while GPIM learns $\pi_\theta(a|\tilde{s}, g)$ by maximizing $\mathcal{I}(s; \omega) + \mathcal{I}(\tilde{s}; \omega)$ without any prior goals and rewards. Here, we characterize the theoretical connection of returns between the two objectives under deterministic π_μ and Assumption 2.

Assumption 2 *The relabeling function f_κ is bijective and the environment is deterministic.*

Let $\eta(\pi_\theta) \triangleq \mathcal{I}(\tilde{s}; g) = \mathbb{E}_{p'(g, \tilde{s}; \theta)} [\log p'(g|\tilde{s}) - \log p'(g)]$, where the expectation is taken over the rollout $p'(g, \tilde{s}; \theta) = p'(g)p(\tilde{s}|g; \theta)$, and $\hat{\eta}(\pi_\theta) \triangleq \mathbb{E}_{p_m^*(\cdot)} [\log p(\omega|\tilde{s}) - \log p(\omega)]$, where the joint distribution $p_m^*(\cdot) \triangleq p(\omega, s, g, \tilde{s}; \mu^*, \kappa, \theta) = p(\omega)p(s|\omega; \mu^*)p(g|s; \kappa)p(\tilde{s}|g; \theta)$, $\mu^* = \arg \max_\mu \mathcal{I}(s; \omega)$, and $\mathbb{E}_{p(\omega, s; \mu^*)} \log p(s|\omega; \mu^*) = 0$. According our training procedure (π_μ is not affected by π_θ) in Algorithm 1, it is trivial to show that $\hat{\eta}(\pi_\theta)$ is a surrogate for our $\mathcal{I}(s; \omega) + \mathcal{I}(\tilde{s}; \omega)$ in Equation 3. We start by deriving that the standard multi-goal RL objective $\eta(\pi_\theta)$ and our (unsupervised) objective $\hat{\eta}(\pi_\theta)$ are equal under some mild assumptions and then generalize this connection to a general case.

Special case: We first assume the prior goal distribution $p'(g)$ for optimizing $\eta(\pi_\theta)$ matches the goal distribution $\mathbb{E}_\omega [p(g|\omega; \mu^*, \kappa)]$ induced by π_{μ^*} and f_κ for optimizing $\hat{\eta}(\pi_\theta)$. Then, we obtain:

$$\begin{aligned} & \hat{\eta}(\pi_\theta) - \eta(\pi_\theta) \\ &= \mathbb{E}_{p_m^*(\cdot)} [\log p(\omega|\tilde{s}) - \log p(\omega) - \log p'(g|\tilde{s}) + \log p'(g)] \\ &= \mathbb{E}_{p_m^*(\cdot)} [\log p(\tilde{s}|\omega; \mu^*, \kappa, \theta) - \log p(\tilde{s}|g; \theta)] = 0. \end{aligned} \quad (9)$$

Equation 9 comes from our relabeling procedure (with deterministic π_{μ^*} and Assumption 2), specifying that $p(\tilde{s}|\omega; \mu^*, \kappa, \theta) = \mathbb{E}_{s, g} [p(s|\omega; \mu^*)p(g|s; \kappa)p(\tilde{s}|g; \theta)]$, $\mathbb{E}_{p_m^*(\cdot)} [\log p(s|\omega; \mu^*)] = 0$ and $\mathbb{E}_{p_m^*(\cdot)} [\log p(g|s; \kappa)] = 0$. Essentially, this special case shows that without inductive bias on the self-generated goal distribution, our learning procedure leads to the desired goal-conditioned policy π_θ .

General case: Suppose that we do not have any prior connection between the goal distributions $p'(g)$ wrt optimizing $\eta(\pi_\theta)$ and the self-generated $\mathbb{E}_\omega [p(g|\omega; \mu^*, \kappa)]$ wrt optimizing $\hat{\eta}(\pi_\theta)$. The following theorem provides such a performance guarantee (Please see appendix for a full derivation):

Theorem 1 *Let $\eta(\pi_\theta)$ and $\hat{\eta}(\pi_\theta)$ be as defined above, and assume relabeling f_κ is bijective, then,*

$$\hat{\eta}(\pi_\theta) - \eta(\pi_\theta) \leq 2R_{max}\sqrt{\epsilon/2},$$

where $R_{max} = \max_{p'(g)p(\tilde{s}|g; \theta)} \log p'(g|\tilde{s}) - \log p'(g)$ and $\epsilon = \mathbb{E}_{p(\omega)} [D_{KL}(p(s|\omega; \mu^*)||p'(s))]$.

This theorem implies that as long as we improve the return wrt $\hat{\eta}(\pi_\theta)$ by more than $2R_{max}\sqrt{\epsilon/2}$, we can guarantee improvement wrt the return $\eta(\pi_\theta)$ of standard multi-goal RL.

Note that the analysis presented above makes an implicit requirement that the goal distribution is valid for training

π_θ (i.e., there is the corresponding target in the environment for the agent to pursue). This requirement is well satisfied for the multi-goal RL. However, ambiguity appears when the goal distribution $\mathbb{E}_\omega [p(g|\omega; \mu^*, \kappa)]$, induced by π_{μ^*} and f_κ , and the existed target $p'(g)$ in the reset environment for training π_θ have different supports. For example, the generated goal is "reaching red square", while such target does not exist in the reset environment for training π_θ (Algorithm 1 *line 14*). Thus, we introduce relabeling over the environment (see appendix) for granting valid training.

4 Related Work

Investigating the goal distribution: For goal-reaching tasks, many prior methods (Schaul et al. 2015; Andrychowicz et al. 2017; Levy et al. 2017; Pong et al. 2018; Hartikainen et al. 2019) assume an available distribution of goals during the exploration. In the unsupervised RL setting, the agent needs to automatically explore the environment and discover potential goals for learning the goal-conditioned policy. Several works (Colas, Sigaud, and Oudeyer 2018; Péré et al. 2018; Warde-Farley et al. 2019; Pong et al. 2019; Kovač, Laversanne-Finot, and Oudeyer 2020) also adopt heuristics to acquire the goal distribution based on previously visited states, which is orthogonal to our relabeling procedure.

Learning the goal-achievement reward function: Building on prior works in standard RL algorithms (Schaul et al. 2015; Schulman et al. 2017; Haarnoja et al. 2018) that learn policies with prior goals and rewards, unsupervised RL faces another challenge — automatically learning the goal-achievement reward function. Two common approaches to obtain rewards are (1) applying *the pre-defined function* on the learned goal representations, and (2) *directly learning a reward function*. Estimating the reward with *the pre-defined function* typically assumes the goal space is the same as the state space, and learns the embeddings of states and goals with various auxiliary tasks (self-supervised loss in perception-level (Hafner et al. 2020)): Sermanet et al. (2018); Warde-Farley et al. (2019); Liu et al. (2021) employ the contrastive loss to acquire embeddings for high-dimensional inputs, and Nair et al. (2018); Florensa et al. (2019); Nair et al. (2019); Pong et al. (2019) elicit the features with the generative models. Over the learned representations, these approaches apply a prior non-parametric measure function (e.g., the cosine similarity) to provide rewards. This contrasts with our decoupled training procedure, where we acquire rewards by scoring current states with their associated latent variables, instead of the perceptual goals. Such procedure provides more flexibility in training the goal-conditioned policy than using pre-defined measurements, especially for the heterogeneous states and goals.

Another approach, *directly learning a reward function*, aims to pursue skills (the latent-conditioned policy) by maximizing the empowerment (Salge, Glackin, and Polani 2014), which draws a connection between option discovery and information theory. This procedure (Achiam et al. 2018; Eysenbach et al. 2018; Gregor, Rezende, and Wierstra 2017; Campos et al. 2020; Sharma et al. 2020; Tian, Liu, and Wang 2020) typically maximizes the mutual information between a latent variable and the induced behav-

iors (states or trajectories), which is optimized by introducing a latent-conditioned reward function. We explicitly relate the states induced by the latent-conditioned policy and reuses the learned discriminator for instructing "imitation".

Hindsight, self-play and knowledge distillation: Our method is similar in spirit to goal relabeling methods like hindsight experience replay (HER) (Andrychowicz et al. 2017) which replays each episode with a different goal in addition to the one the agent was trying to achieve. By contrast, our GPIM relabels the task for another policy while keeping behavior invariant. The self-play (Sukhbaatar et al. 2017, 2018) and knowledge distillation (Xu et al. 2020) are also related to our relabeling scheme, aiming to refine the training of one task with another associated task.

5 Experiments

Extensive experiments are conducted to evaluate our proposed GPIM method, where the following four questions will be considered in the main paper: (1) By using the "archery" task, we clarify whether q_ϕ can provide an effective reward function on learning the goal-conditioned policy π_θ . Furthermore, more complex tasks including navigation, object manipulation, atari games, and mujoco tasks are introduced to answer: (2) Does our model learn effective behaviors conditioned on a variety of goals (with different procedural relabeling f_κ), including high-dimensional images and text descriptions that are heterogeneous to states? (3) Does the proposed GPIM on learning the goal-conditioned policy outperform baselines? (4) Does the learned reward function produce better expressiveness of tasks, compared to the prior non-parametric function in the embedding space? For more experimental questions, analysis and results, see Appendix 7 and <https://sites.google.com/view/gpim> (video).

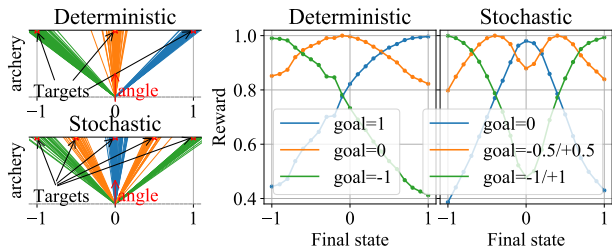


Figure 3: "Archery" tasks (left) and the learned rewards (right) on both deterministic and stochastic environments.

Visualizing the learned reward function. We start with simple "archery" task to visualize how the learned reward function (discriminator q_ϕ) accounts for goal-conditioned behaviors in environment. The task shown in Figure 3 requires choosing an angle at which we shoot an arrow to the target. The left upper subfigure shows that in a deterministic environment, given three different but fixed targets (with different colors), the arrow reaches the corresponding target successfully under the learned reward function q_ϕ . The reward as a function of the final location of arrows in three tasks is shown on the right. We can find that the learned reward functions resemble convex in terms of the distance

between final states to targets. Specifically, the maximum value of the learned reward function is achieved when the final state is close to the given target. The farther away the agent's final state is from the target, the smaller this reward value is. Similarly, the same conclusion can be drawn from the stochastic environment in the left lower subfigure, where the angle of the arrow has a 50% chance to become a mirror symmetric angle. We see that the learned reward function substantially describes the environment's dynamics and the corresponding tasks, both in deterministic and stochastic environments. This answers our *first* question.

Scaling to more complex tasks. To answer our *second* question, we now consider more complex tasks as shown in Figure 4. (1) In *2D navigation tasks*, an agent can move in each of the four cardinal directions. We consider the following two tasks: moving the agent to a specific coordinate named *x-y goal* (see appendix for details) and moving the agent to a specific object with certain color and shape named *color-shape goal*. (2) *Object manipulation* considers a moving agent in 2D environment with one block for manipulation, and the other block as a distractor. The agent first needs to reach the block and then move the block to the target location, where the block is described using color and shape. In other words, the description of the goal contains the *color-shape goal* of the true block and the *x-y goal* of the target coordinate. (3) Three *atari games* including *seaquest*, *berzerk* and *montezuma revenge* require an agent to reach the given final states. (4) We use three *mujoco tasks* (*swimmer*, *half cheetah*, and *fetch*) taken from OpenAI GYM (Brockman et al. 2016) to fast imitate given expert trajectories. Specifically, the *static* goals for π_θ in 2D navigation, object manipulation and atari games are the relabeled final state s_T induced by the latent-conditioned policy π_μ : $g_t = f_\kappa(s_T)$, and the *dynamic* goals for π_θ in mujoco tasks are the relabeled states induced by π_μ at each time step: $g_t = f_\kappa(s_{t+1})$ for $0 \leq t \leq T - 1$.

The left subfigure of Figure 4(a) shows the learned behavior of navigation in continuous action space given the x-y goal which is denoted as the small circle, and the right subfigure shows the trajectory of behavior with the given color-shape goal. As observed, the agent manages to learn navigation tasks by using GPIM. Further, 2D navigation with color-shape goal (Figure 4(a) *right*) and object manipulation tasks (Figure 4(b)) show the effectiveness of our model facing heterogeneous goals and states. Specifically, Figure 4(b) shows the behaviors of the agent on object manipulation, where the agent is asked to first arrive at a block (i.e., blue circle and green square respectively) and then push it to the target location inside a dark circle (i.e., [6.7, 8.0] and [4.8, 7.9] respectively), where the red object exists as a distractor. Figure 4(c) shows the behaviors of agents that reach the final states in a higher dimensional (action, state and goal) space on *seaquest* and *montezuma revenge* respectively. Figure 4(d-e) shows how the agent imitates expert trajectories (dynamic goals) of *swimmer* and *half cheetah*. We refer the reader to appendix for more results (task *berzerk* and *fetch*).

By learning to reach diverse goals generated by the latent-conditioned policy and employing the self-supervised loss over the perception-level to represent goals, the agent learns

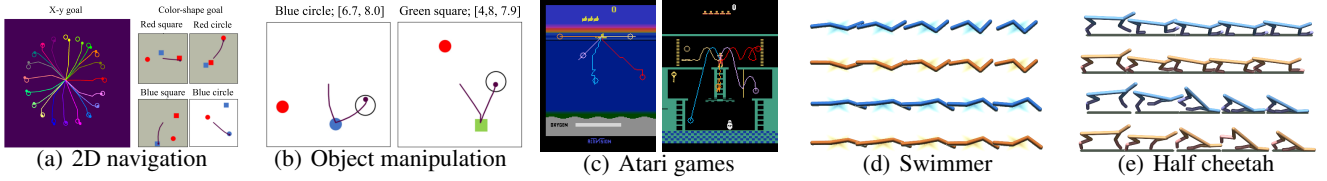


Figure 4: Goals and learned behaviors: Dots in 2D navigation (x-y goal) and atari games denote different final (*static*) goal states, and curves with same color represent corresponding trajectories; Goals in 2D navigation (color-shape goal) and object manipulation are described using the text at the top of the diagram, where the purple lines imply the behaviors; In the swimmer and half cheetah tasks, the first and third rows represent the *dynamic* goals, and each row below represents the learned behaviors.

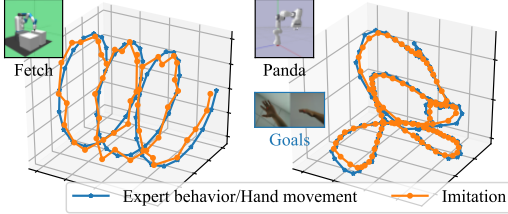


Figure 5: Dynamic goals on Fetch and Panda.

the ability to infer new goals later encountered by the agent. For example, as in Figure 4(a) (*right*), learning three behaviors with the goal of red-square, red-circle or blue-square (gray background) makes the agent accomplish the new goal of blue-circle (white background). In appendix, we also conduct the ablation study to show how the self-supervised loss (in the perception-level) affects behaviors, and provide more experiments to show the generalization to unseen goals.

Compared to the usual relabeling procedure (e.g., HER with static goals) or latent variable base methods (e.g., DIAYN, equivalent to $f_{\kappa} = q_{\phi}$ in our GPIM), our approach scales to dynamic goals. Considering the setting of dynamic relabeling in *fetch* task, we further demonstrate the ability of GPIM on temporally-extended tasks, where the 3D-coordinates of the gripper of the robotic arm is relabeled as goals for "imitation" in the training phase. During test, we employ a parameterized complex curve, $(x, y, z) = (t/5, \cos(t)/5 - 1/5, \sin(t)/5)$, for the gripper to follow and show their performance in Figure 5 (left). It is worth noting that during training the agent is required to imitate a large number of simple behaviors and has never seen such complex goals before testing. We also validate GPIM on a Franka Panda robot (Figure 5 right)), purposing tracking of hand movement, with MediaPipe (Lugaresi et al. 2019) to capturing features of images. It is observed from Figure 5 that the imitation curves are almost overlapping with the given desired trajectories, indicating that the agent using GPIM framework has the potential to learn such compositional structure of goals during training and generalize to new composite goals during test.

Comparison with baselines. For the *third* question, we mainly compare our method to three baselines: **RIG** (Nair et al. 2018), **DISCERN** (Warde-Farley et al. 2019), and **L2 Distance**. L2 Distance measures the distance between states

and goals, where the L2 distance $-||\tilde{s}_{t+1} - g_t||^2 / \sigma_{pixel}$ is considered with a hyperparameter σ_{pixel} . Note that 2D navigation with the color-shape goal and object manipulation using text description makes the dimensions of states and goals different, so L2 cannot be used in these two tasks. In RIG, we obtain rewards by using the distances in two embedding spaces and learning two independent VAEs, where one VAE is to encode states and the other is to encode goals. For this heterogeneous setting, we also conduct baseline **RIG⁺** by training one VAE only on goals and then reward agent with the distance between the embeddings of goals and relabeled states (i.e., g_t vs. $f_{\kappa}(\tilde{s}_{t+1})$). We use the normalized distance to goals as the evaluation metric, where we generate 50 goals (tasks) as validation.

We show the results in Figure 6 by plotting the normalized distance to goals as a function of the number of actor's steps, where each curve considers 95% confidence interval in terms of the mean value across three seeds. As observed, our GPIM consistently outperforms baselines in almost all tasks except for the RIG in 2D navigation (x-y goal) due to the simplicity of this task. Particularly, as the task complexity increases from 2D navigation (x-y goal) to 2D navigation (color-shape goal) and eventually object manipulation (mixed x-y goal and color-shape goal), GPIM converges faster than baselines and the performance gap between our GPIM and baselines becomes larger. Moreover, although RIG learns fast on navigation with x-y goal, it fails to accomplish complex navigation with color-shape goal because the embedding distance between two independent VAEs has difficulty in capturing the correlation of heterogeneous states and goals. Even with a stable VAE, RIG⁺ can be poorly suited for training the goal-reaching policy. Especially in high-dimensional action space and on more exploratory tasks (atari and mujoco tasks), our method substantially outperforms the baselines.

To gain more intuition for our method, we record the distance (Δd) between the goal induced by π_{μ} and the final state induced by π_{θ} throughout the training process of the 2D navigation (x-y goal). In this specific experiment, we update π_{μ} and q_{ϕ} but ignore the update of π_{θ} before 200 k steps to show the exploration of π_{μ} at the task generation phase. As shown in Figure 7, Δd steadily increases during the first 200 k steps, indicating that the latent-conditioned policy π_{μ} explores the environment (i.e., goal space) to distinguish skills more easily (with q_{ϕ}), and as a result, gen-

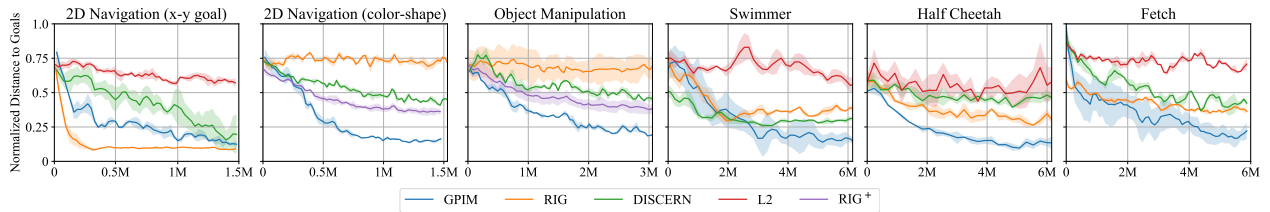


Figure 6: Performance (normalized distance to goals vs. actor steps) of our GPIM and baselines (RIG, DISCERN, L2, RIG+).

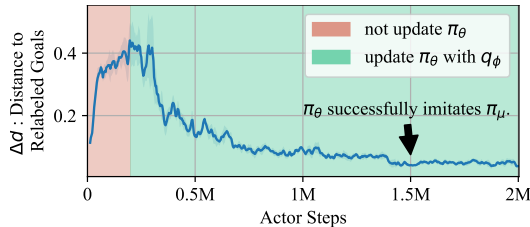


Figure 7: *Pink slice*: Latent-conditioned π_μ gradually explores environment, generating more difficult goals. *Mint green*: Learned discriminator q_ϕ encourages π_θ to mimic π_μ .

erates diverse goals for training goal-conditioned policy π_θ . After around 1.5 M steps, Δd almost comes to 0, indicating that goal-conditioned π_θ has learned a good strategy to reach the relabeled goals. In appendix, we visually show the generated goals in more complex tasks, which shows that our straightforward framework can effectively explore without additional sophisticated exploration strategies.

Expressiveness of the reward function. Particularly, the performance of unsupervised RL methods depend on the diversity of generated goals and the expressiveness of the learned reward functions that are conditioned on the goals. We show that our straightforward framework can effectively explore environments in appendix (though it is not our focus). The next question is that: with the same exploration capability to generate goals, does our model achieve competitive performance against the baselines? Said another way, will the obtained rewards (over embedding space) of baselines taking prior non-parametric functions limit the repertoires of learning tasks in some environments? For better graphical interpretation and comparison with baselines, we simplify the complex Atari games to a maze environment shown in Figure 8, where the middle wall poses a bottleneck state. At the same time, as an example to show the compatibility of our objective with existing exploration strategies (Jabri et al. 2019; Lee et al. 2019), we set the reward for the latent-conditioned policy π_μ as $r'_t = \lambda r_t + (\lambda - 1) \log q_\nu(s_{t+1})$, where q_ν is a density model, and $\lambda \in [0, 1]$ can be interpreted as trade off between discriminability of skills and task-specific exploration (here we set $\lambda = 0.5$). Note that we modify r'_t for improving the exploration on generating goals and we do not change the reward for training goal-conditioned π_θ . To guarantee the generation of same diverse goals for goal-conditioned policies of baselines, we adopt π_μ taking the modified r'_t to generate goals for RIG and DISCERN.

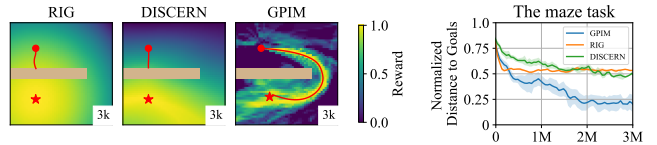


Figure 8: (Left) Reward functions, where heatmaps depict the reward conditioned on the bottom-left goal, reaching the left-bottom star. (Right) Learning curves on the left maze.

In Figure 8, we visualize the learned reward on a specific task reaching the left-bottom star, and the learning curves on the maze task, where the testing-goals are random sampled. We can see that the learned rewards of RIG and DISCERN produce poor signal for the goal-conditioned policy, which makes learning vulnerable to local optima. Our method acquires the reward function q_ϕ after exploring the environment, dynamics of which itself further shapes the reward function. In Figure 8 (left), we can see that our model provides the reward function better expressiveness of the task by compensating for the dynamics of training environment. This produces that, even with the same exploration capability to generate diverse goals, our model sufficiently outperforms the baselines, as shown in Figure 8 (right).

6 Conclusion

In this paper, we propose GPIM to learn a goal-conditioned policy in an unsupervised manner. The core idea of GPIM lies in that we introduce a latent-conditioned policy with a procedural relabeling procedure to generate tasks (goals and the associated reward functions) for training the goal-conditioned policy. For goal-reaching tasks, we theoretically describe the performance guarantee of our (unsupervised) objective compared with the standard multi-goal RL. We also conduct extensive experiments on a variety of tasks to demonstrate the effectiveness and efficiency of our method.

There are several potential directions for future in our unsupervised relabeling framework. One promising direction would be developing a domain adaptation mechanism when the interaction environments (action/state spaces, dynamics, or initial states) wrt learning π_μ and π_θ are different. Additionally, GPIM can get benefits from more extensive exploration strategies to control the exploration-exploitation trade-off. Finally, latent-conditioned π_μ (generating goals and reward functions) is not affected by the goal-conditioned π_θ in GPIM. One can develop self-paced (curriculum) learning over the two policies under the unsupervised RL setting.

Acknowledgments

The authors would like to thank Yachen Kang for helpful discussions and the anonymous reviewers for the valuable comments. This work is supported by NSFC General Program (62176215).

References

- Achiam, J.; Edwards, H.; Amodei, D.; and Abbeel, P. 2018. Variational Option Discovery Algorithms. *CoRR*, abs/1807.10299.
- Amodei, D.; Olah, C.; Steinhardt, J.; Christiano, P. F.; Schulman, J.; and Mané, D. 2016. Concrete problems in AI safety. *CoRR*, abs/1606.06565.
- Andrychowicz, M.; Wolski, F.; Ray, A.; Schneider, J.; Fong, R.; Welinder, P.; McGrew, B.; Tobin, J.; Abbeel, O. P.; and Zaremba, W. 2017. Hindsight experience replay. In *Advances in neural information processing systems*, 5048–5058.
- Badia, A. P.; Piot, B.; Kapturowski, S.; Sprechmann, P.; Vitvitskyi, A.; Guo, D.; and Blundell, C. 2020. Agent57: Outperforming the atari human benchmark. *arXiv preprint arXiv:2003.13350*.
- Barber, D.; and Agakov, F. V. 2003. The IM algorithm: a variational approach to information maximization. In *Advances in neural information processing systems*, None.
- Beaudry, N. J.; and Renner, R. 2011. An intuitive proof of the data processing inequality. *arXiv preprint arXiv:1107.0740*.
- Berner, C.; Brockman, G.; Chan, B.; Cheung, V.; Debiak, P.; Dennison, C.; Farhi, D.; Fischer, Q.; Hashme, S.; Hesse, C.; et al. 2019. Dota 2 with large scale deep reinforcement learning. *arXiv preprint arXiv:1912.06680*.
- Brockman, G.; Cheung, V.; Pettersson, L.; Schneider, J.; Schulman, J.; Tang, J.; and Zaremba, W. 2016. OpenAI Gym. .
- Campos, V. A.; Trott, A.; Xiong, C.; Socher, R.; i Nieto, X. G.; and Torres, J. 2020. Explore, Discover and Learn: Unsupervised Discovery of State-Covering Skills. *ArXiv*, abs/2002.03647.
- Colas, C.; Karch, T.; Lair, N.; Dussoux, J.; Moulin-Frier, C.; Dominey, P. F.; and Oudeyer, P. 2020. Language as a Cognitive Tool to Imagine Goals in Curiosity Driven Exploration. In Larochelle, H.; Ranzato, M.; Hadsell, R.; Balcan, M.; and Lin, H., eds., *Advances in Neural Information Processing Systems 33: Annual Conference on Neural Information Processing Systems 2020, NeurIPS 2020, December 6-12, 2020, virtual*.
- Colas, C.; Sigaud, O.; and Oudeyer, P.-Y. 2018. Gep-pg: Decoupling exploration and exploitation in deep reinforcement learning algorithms. *arXiv preprint arXiv:1802.05054*.
- Eysenbach, B.; Gupta, A.; Ibarz, J.; and Levine, S. 2018. Diversity is all you need: Learning skills without a reward function. *arXiv preprint arXiv:1802.06070*.
- Florensa, C.; Degraeve, J.; Heess, N.; Springenberg, J. T.; and Riedmiller, M. 2019. Self-supervised learning of image embedding for continuous control. *arXiv preprint arXiv:1901.00943*.
- Gregor, K.; Rezende, D. J.; and Wierstra, D. 2017. Variational Intrinsic Control.
- Gupta, A.; Eysenbach, B.; Finn, C.; and Levine, S. 2018. Unsupervised Meta-Learning for Reinforcement Learning. *CoRR*, abs/1806.04640.
- Haarnoja, T.; Zhou, A.; Abbeel, P.; and Levine, S. 2018. Soft actor-critic: Off-policy maximum entropy deep reinforcement learning with a stochastic actor. *arXiv preprint arXiv:1801.01290*.
- Hafner, D.; Ortega, P. A.; Ba, J.; Parr, T.; Friston, K. J.; and Heess, N. 2020. Action and Perception as Divergence Minimization. *CoRR*, abs/2009.01791.
- Hartikainen, K.; Geng, X.; Haarnoja, T.; and Levine, S. 2019. Dynamical Distance Learning for Semi-Supervised and Unsupervised Skill Discovery. In *International Conference on Learning Representations*.
- Higgins, I.; Pal, A.; Rusu, A.; Matthey, L.; Burgess, C.; Pritzel, A.; Botvinick, M.; Blundell, C.; and Lerchner, A. 2017. Darla: Improving zero-shot transfer in reinforcement learning. In *Proceedings of the 34th International Conference on Machine Learning-Volume 70*, 1480–1490. JMLR.org.
- Jabri, A.; Hsu, K.; Gupta, A.; Eysenbach, B.; Levine, S.; and Finn, C. 2019. Unsupervised curricula for visual meta-reinforcement learning. In *Advances in Neural Information Processing Systems*, 10519–10531.
- Khrodar, R.; Yoo, D.; and Kitani, K. M. 2018. VADRA: Visual adversarial domain randomization and augmentation. *arXiv preprint arXiv:1812.00491*.
- Kovač, G.; Laversanne-Finot, A.; and Oudeyer, P.-Y. 2020. Grimgap: learning progress for robust goal sampling in visual deep reinforcement learning. *arXiv preprint arXiv:2008.04388*.
- Laskin, M.; Srinivas, A.; and Abbeel, P. 2020. CURL: Contrastive Unsupervised Representations for Reinforcement Learning. 119: 5639–5650.
- Lee, L.; Eysenbach, B.; Parisotto, E.; Xing, E. P.; Levine, S.; and Salakhutdinov, R. 2019. Efficient Exploration via State Marginal Matching. *CoRR*, abs/1906.05274.
- Lee, Y.; Sun, S.-H.; Somasundaram, S.; Hu, E. S.; and Lim, J. J. 2018. Composing complex skills by learning transition policies. In *International Conference on Learning Representations*.
- Levy, A.; Konidaris, G.; Platt, R.; and Saenko, K. 2017. Learning multi-level hierarchies with hindsight. *arXiv preprint arXiv:1712.00948*.
- Liu, G.; Zhang, C.; Zhao, L.; Qin, T.; Zhu, J.; Li, J.; Yu, N.; and Liu, T. 2021. Return-Based Contrastive Representation Learning for Reinforcement Learning. *CoRR*, abs/2102.10960.
- Lowrey, K.; Rajeswaran, A.; Kakade, S. M.; Todorov, E.; and Mordatch, I. 2019. Plan Online, Learn Offline: Efficient Learning and Exploration via Model-Based Control.
- Lu, X.; Lee, K.; Abbeel, P.; and Tiomkin, S. 2020. Dynamics Generalization via Information Bottleneck in Deep Reinforcement Learning. *CoRR*, abs/2008.00614.

- Lugaresi, C.; Tang, J.; Nash, H.; McClanahan, C.; Uboweja, E.; Hays, M.; Zhang, F.; Chang, C.; Yong, M. G.; Lee, J.; Chang, W.; Hua, W.; Georg, M.; and Grundmann, M. 2019. MediaPipe: A Framework for Building Perception Pipelines. *CoRR*, abs/1906.08172.
- Nair, A.; Bahl, S.; Khazatsky, A.; Pong, V.; Berseth, G.; and Levine, S. 2019. Contextual Imagined Goals for Self-Supervised Robotic Learning. 100: 530–539.
- Nair, A. V.; Pong, V.; Dalal, M.; Bahl, S.; Lin, S.; and Levine, S. 2018. Visual reinforcement learning with imagined goals. In *Advances in Neural Information Processing Systems*, 9191–9200.
- Péré, A.; Forestier, S.; Sigaud, O.; and Oudeyer, P.-Y. 2018. Unsupervised learning of goal spaces for intrinsically motivated goal exploration. *arXiv preprint arXiv:1803.00781*.
- Pitis, S.; Chan, H.; Zhao, S.; Stadie, B. C.; and Ba, J. 2020. Maximum Entropy Gain Exploration for Long Horizon Multi-goal Reinforcement Learning. *ArXiv*, abs/2007.02832.
- Pong, V.; Gu, S.; Dalal, M.; and Levine, S. 2018. Temporal difference models: Model-free deep rl for model-based control. *arXiv preprint arXiv:1802.09081*.
- Pong, V. H.; Dalal, M.; Lin, S.; Nair, A.; Bahl, S.; and Levine, S. 2019. Skew-fit: State-covering self-supervised reinforcement learning. *arXiv preprint arXiv:1903.03698*.
- Popov, I.; Heess, N.; Lillicrap, T.; Hafner, R.; Barth-Maron, G.; Vecerik, M.; Lampe, T.; Tassa, Y.; Erez, T.; and Riedmiller, M. 2017. Data-efficient deep reinforcement learning for dexterous manipulation. *arXiv preprint arXiv:1704.03073*.
- Salge, C.; Glackin, C.; and Polani, D. 2014. Empowerment—an introduction. In *Guided Self-Organization: Inception*, 67–114. Springer.
- Schaul, T.; Horgan, D.; Gregor, K.; and Silver, D. 2015. Universal value function approximators. In *International conference on machine learning*, 1312–1320.
- Schulman, J.; Wolski, F.; Dhariwal, P.; Radford, A.; and Klimov, O. 2017. Proximal Policy Optimization Algorithms. *CoRR*, abs/1707.06347.
- Sermanet, P.; Lynch, C.; Chebotar, Y.; Hsu, J.; Jang, E.; Schaal, S.; Levine, S.; and Brain, G. 2018. Time-contrastive networks: Self-supervised learning from video. In *2018 IEEE International Conference on Robotics and Automation (ICRA)*, 1134–1141. IEEE.
- Sharma, A.; Gu, S.; Levine, S.; Kumar, V.; and Hausman, K. 2020. Dynamics-Aware Unsupervised Discovery of Skills.
- Sukhbaatar, S.; Denton, E.; Szlam, A.; and Fergus, R. 2018. Learning goal embeddings via self-play for hierarchical reinforcement learning. *arXiv preprint arXiv:1811.09083*.
- Sukhbaatar, S.; Lin, Z.; Kostrikov, I.; Synnaeve, G.; Szlam, A.; and Fergus, R. 2017. Intrinsic motivation and automatic curricula via asymmetric self-play. *arXiv preprint arXiv:1703.05407*.
- Tian, Q.; Liu, J.; and Wang, D. 2020. Learning transitional skills with intrinsic motivation.
- Tobin, J.; Fong, R.; Ray, A.; Schneider, J.; Zaremba, W.; and Abbeel, P. 2017. Domain randomization for transferring deep neural networks from simulation to the real world. In *2017 IEEE/RSJ International Conference on Intelligent Robots and Systems (IROS)*, 23–30. IEEE.
- Todorov, E.; Erez, T.; and Tassa, Y. 2012. MuJoCo: A physics engine for model-based control. In *2012 IEEE/RSJ International Conference on Intelligent Robots and Systems, IROS 2012, Vilamoura, Algarve, Portugal, October 7-12, 2012*, 5026–5033. IEEE.
- Vecerik, M.; Sushkov, O.; Barker, D.; Rothörl, T.; Hester, T.; and Scholz, J. 2019. A practical approach to insertion with variable socket position using deep reinforcement learning. In *2019 International Conference on Robotics and Automation (ICRA)*, 754–760. IEEE.
- Warde-Farley, D.; de Wiele, T. V.; Kulkarni, T. D.; Ionescu, C.; Hansen, S.; and Mnih, V. 2019. Unsupervised Control Through Non-Parametric Discriminative Rewards. In *7th International Conference on Learning Representations, ICLR 2019, New Orleans, LA, USA, May 6-9, 2019*. Open-Review.net.
- Xu, G.; Liu, Z.; Li, X.; and Loy, C. C. 2020. Knowledge Distillation Meets Self-Supervision. *arXiv preprint arXiv:2006.07114*.
- Zhang, J.; Yu, H.; and Xu, W. 2021. Hierarchical Reinforcement Learning By Discovering Intrinsic Options. *CoRR*, abs/2101.06521.

Appendix

Here, we will provide additional experiments (Section 7), theoretical derivations (Section 8), implementation details (Section 9), and more results with respect the experiments in the main text (Section 10).

7 Additional Experiments

In this section, we make the additional experiments to

- (7.1) compare our method with DIAYN and its variant,
- (7.2) show the generalization when the dynamics and goal conditions are missing,
- (7.3) conduct the ablation study to analyze how the self-supervised loss over the perception-level affects the learned behaviors in terms of the generalization to new tasks,
- (7.4) explore the (automatic) goal distribution generation,
- (7.5) analyze the effect caused by the underspecified latent (support) space,
- (7.6) lift the Assumption 1 (assuming fixed initial state) in the main text,
- (7.7) evaluate the robustness of GPIM on stochastic MDP (with varying stochasticity).

7.1 Comparison with DIAYN and its Variant

In this section, we expect to clarify the difference and connection with DIAYN (Eysenbach et al. 2018) experimentally, and indicate the limitations of maximizing $\mathcal{I}(s; \omega)$ and maximizing $\mathcal{I}(s; g)$ separately in learning the goal-conditioned policy.

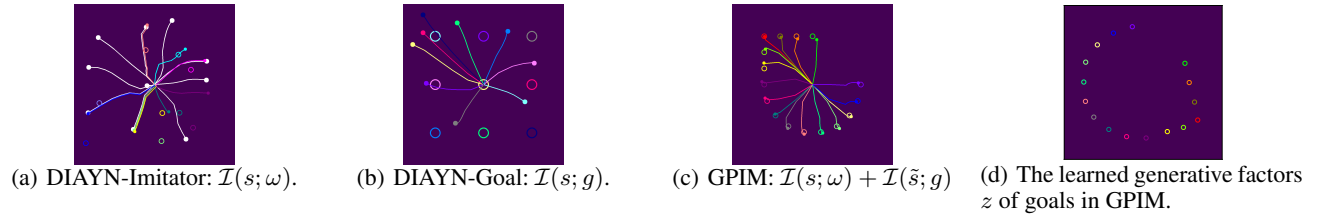


Figure 9: 2D navigation with (a) DIAYN-Imitator, (b) DIAYN-Goal, and (c) our proposed GPIM. In (a), (b) and (c), the open (colored) circle denotes the user-specified goal in test, and the (colored) line with a solid circle at the end is the corresponding behavior. Note that the white lines in (a) are the learned skills in the training process, where we show 10 diverse skills. We can see that neither DIAYN-Imitator nor DIAYN-Goal approaches the corresponding goals, while our model succeeds in reaching the goal as shown in (c). In (d), we also show the generative factors z (see Figure 12 in section 7.3) by disentangling goals with the self-supervised loss over the perception-level in (d), where the open circles with different colors in (d) correspond to the goals in (c).

In DIAYN, authors show the ability of the model to imitate an expert. Given the goal, DIAYN uses the learned discriminator to estimate which skill was most likely to have generated the goal g :

$$\hat{\omega} = \arg \max_{\omega} q_{\phi}(\omega|g). \quad (10)$$

Here we call this model *DIAYN-Imitator*. We also directly substitute the perceptually-specific goals for the latent variable in DIAYN’s objective to learn a goal-conditioned policy. We call this model *DIAYN-Goal*:

$$\max \mathcal{I}(s; g), \quad (11)$$

where g is sampled from the prior goal distribution $p(g)$. Please note that we do not adopt the prior non-parametric distance as in DISCERN (Warde-Farley et al. 2019) to calculate the reward. We obtain the reward as in vanilla DIAYN using the variational approximator $q_{\phi}(g|s)$.

Figure 9 shows the comparison of our GPIM with DIAYN variants, including DIAYN-Imitator and DIAYN-Goal, where the 2D navigation task is considered. As observed, DIAYN-Imitator can reach seen goals in training (white lines) but not unseen goals in test in Figure 9(a), because it cannot effectively accomplish the interpolation between skills that are induced in training. And behaviors generated by DIAYN-Goal cannot guarantee consistency with the preset goals in Figure 9(b). The main reason is that such objective only ensures that when g (or ω) is different, the states generated by g (or ω) are different. However, there is no guarantee that g (or ω) and the state generated by the current g (or ω) keep semantically consistent. Our proposed GPIM method, capable of solving interpolation and consistency issues, exhibits the best performance in this 2D navigation task.

Moreover, when the user-specified goals are heterogeneous to the states, the learned discriminator q_{ϕ} in DIAYN is unable to estimate which skill is capable of inducing given goals. Specifically, when goals are visual inputs, and states in training is

feature vectors (e.g., joint angles), the learned discriminator is unable to choose the skills due to a lack of models for converting high-dimensional images into low-dimensional feature vectors. On the contrary, there are lots of off-the-shelf models to render low-dimensional feature vectors into perceptually-specific high-dimensional inputs (Tobin et al. 2017; Khirdkar, Yoo, and Kitani 2018).

7.2 Generalization on the Gridworld Task

Here we introduce an illustrative example of gridworld task and then show the generalization when the dynamics and goal conditions are missing in the gridworld task.

Illustrative example. Here, we start with a simple gridworld example: the environment is shown on the left of Figure 10, where the goal for the agent is to navigate from the middle to the given colored room. By training the latent-conditioned policy and the discriminator, our method quickly acquires four skills ($\omega = 1000; 0100; 0010; 0001$) to reach different rooms. Each time the agent arrives in a room induced by π_μ , we train π_θ conditioned on the room’s color (e.g., green), allowing the agent to be guided to the same room by the current reward function (e.g. q_ϕ conditioned on $\omega = 1000$). The results are shown on the right of Figure 10, where the upper and lower subfigures show the learning processes of latent-conditioned policy π_μ and goal-conditioned policy π_θ respectively. It is concluded that the agent can automatically learn how to complete tasks given semantic goals in an unsupervised manner.

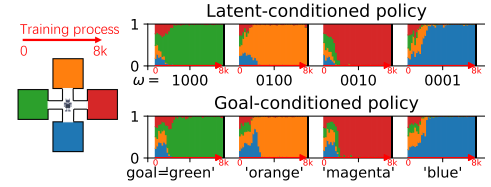


Figure 10: Gridworld tasks. Y-axis is the percentage of different rooms that the robot arrives in.

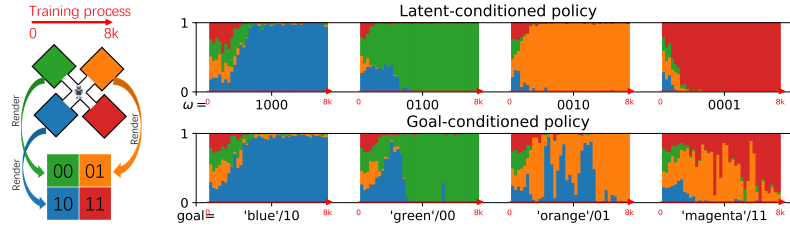


Figure 11: Gridworld tasks. The Y-axis is the percentage of different rooms that agent arrives in.

Generalization on the gridworld task. We further show the generalization when the dynamics and goal conditions are missing in the gridworld task, where there are four rooms in different colors: blue, green, orange and magenta. We consider the situation where we train the goal-conditioned policy in the blue room, the green room and the orange room, and test in the magenta room.

As shown in Figure 11, we quickly acquire four skills for different rooms through the training at the abstract level. After the agent reaches at the colored rooms, we relabel the corresponding room as a two-bit representation: $f_\kappa('blue') = 10$, $f_\kappa('green') = 00$, and $f_\kappa('orange') = 01$; we do not relabel the magenta room. We take the magenta room corresponding to 11 as the test goal to verify the generalization ability.

In lower part of Figure 11, we show the learning process of the goal-conditioned policy. We can find that the blue room task is completed quickly, and the green and orange room tasks are learned relatively slowly, and the agent is still able to complete the (new) test task successfully (the magenta room). Compared to the task in Figure 10 that relabel all the rooms as goals, the whole learning process in Figure 11 is much slower. We hypothesize that the main reason is that the agent needs to further infer the relationship between different goals. The lack of goal information (i.e., missing magenta 11) leads to a lower efficiency and unstable training.

7.3 Self-Supervised Loss over the Perception-Level

As indicated by Laskin, Srinivas, and Abbeel (2020), control algorithms built on top of useful semantic representations should be significantly more efficient. We further optimize the goal-conditioned policy π_θ with an associated self-supervised loss on the perception-level, so as to improve the learning efficiency and generalization ability of the goal-conditioned policy π_θ facing high-dimensional goals. As shown in Figure 12, we decompose π_θ into two components: the encoder network E parameterized by ϑ_E and the generative network G parameterized by ϑ_G . Hence, we optimize the overall objective function for the goal-

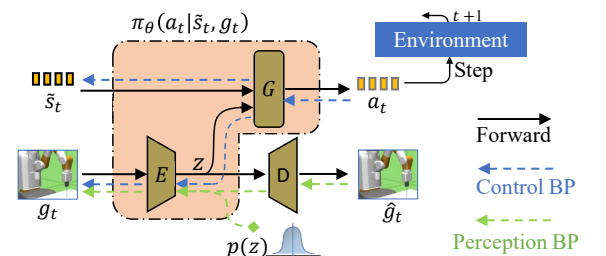


Figure 12: Optimization for the goal-conditioned policy π_θ with the control-level loss (SAC with reward \tilde{r}_t) and perception-level loss.

conditioned policy π_θ :

$$\max_{\vartheta_E, \vartheta_G, \vartheta_D} \mathbb{E}_{p_m(\cdot)} [\log q_\phi(\omega|\tilde{s})] + Prec_loss, \quad (12)$$

where the self-supervised loss on the perception-level $Prec_loss$ includes the reconstruction loss and a prior matching loss (with an isotropic unit Gaussian prior $p(z) = N(0; I)$):

$$Prec_loss \triangleq \underbrace{\alpha \cdot \mathbb{E}_{p(g)p_{\vartheta_E}(z|g)} [p_{\vartheta_D}(g|z)]}_{\text{reconstruction loss}} - \underbrace{\beta \cdot \mathbb{E}_{p(g)} [KL(q_{\vartheta_E}(z|g)||p(z))]}_{\text{prior matching loss}},$$

where $p(g) = p(\omega)p(s|\omega; \mu)p(g|s; \kappa)$, α and β are two hyperparameters. It is worth noting that the update of the encoder E is based on gradients from both π_θ and $Prec_loss$.

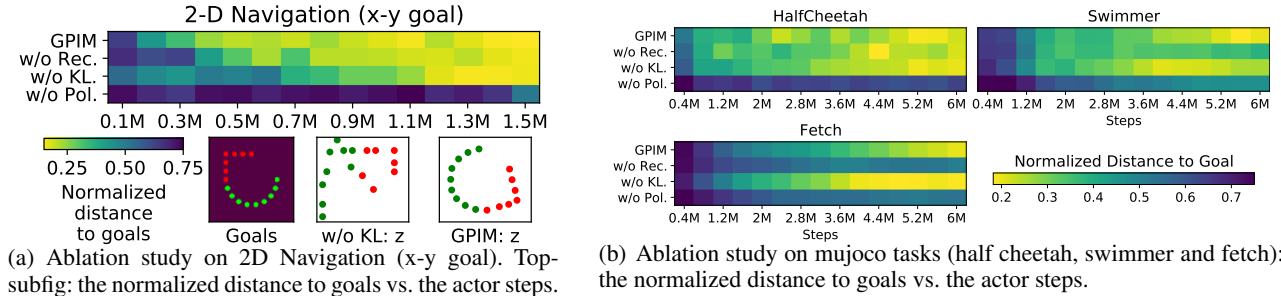


Figure 13: Ablation studies for the perception loss.

Ablation study on 2D navigation. Here we conduct the ablation study on 2D navigation task to analyze how the perception-level loss in GPIM affects the learned behaviors in terms of the generalization to new tasks. For convenience, we remove certain component from GPIM and define the new method as follows: *w/o Rec* - removing the reconstruction loss (i.e. $\alpha = 0$); *w/o KL* - removing the KL loss (i.e. $\beta = 0$); *w/o Pol* - removing the policy loss updating ϑ_E as shown in Figure 12.

The performance is reported in Figure 13(a). It is observed that *w/o Pol* performs worse than all other methods, which is consistent with the performance of RIG that trains VAE and policy separately. The main reason is that the perception-level loss fails to figure out the required latent factors on given tasks. Moreover, although GPIM has a similar performance with the other three methods on 2D navigation task, GPIM has better interpretability to behaviors. As shown in Figure 13(a) (bottom), considering a series of goals from the first red to the last green (left) in a counterclockwise order, GPIM can successfully disentangle them and learn effective latent z (right), but *w/o KL* fails to keep the original order of goals (middle).

Ablation study on mujoco tasks. We further study the impact of perception-level loss on mujoco tasks. The performance is reported in Figure 13(b). It is observed that *w/o Pol* performs worse than all other methods, which is consistent with the performance in 2D navigation task. And we can find that when we remove the reconstruction loss ($\alpha = 0$), the performance of *w/o Rec* degrades in these three environments. The main reason is that the process of learning generative factors become more difficult without the supervised reconstruction loss. While in 2D navigation task, the reconstruction loss has little impact on the performance. Even though that *w/o KL* has a similar performance with our full GPIM method, GPIM demonstrates better interpretability to behaviors as shown in Figure 9(d).

7.4 Automated Goal-Generation for Exploration

In general, for unsupervised RL, we would like to ask the agent to carry out autonomous "practice" during training phase, where we do not know which particular goals will be provided in test phase. In order to maximize the state coverage, the ability to automatically explore the environment and discover diverse goals is crucial. In this section, we will further analyze the goal distribution of three methods (RIG (Nair et al. 2018), DISCERN (Warde-Farley et al. 2019), GPIM) in a new 2D obstacle navigation task as shown in Figure 14(a), Figure 14(b), and Figure 14(c). The size of the environment is 10×10 , the initial state is set as $[5, 2]$, and there are two obstacles that prevent the agent from passing through each of which is 3×6 in size.

DISCERN samples goals during training by maintaining a fixed sized buffer \mathcal{G} of past observations. We simply mimic the process of goal generation by taking random actions for 20 environment steps. As in Figure 14(b), we generate 100 goals with different colors. We can see that the majority of goals locate between the two obstacles, which limits the further exploration of the environment.

RIG samples a representation (latent goals z_g) from the learned VAE prior, which represents a distribution over latent goals. The policy network takes the representation as a substitute for the user-specified goal. For a clear visualization of the distribution of the sampled latent goals, we further feed the sampled latent goals into the decoder to obtain the real goals in the user-specified

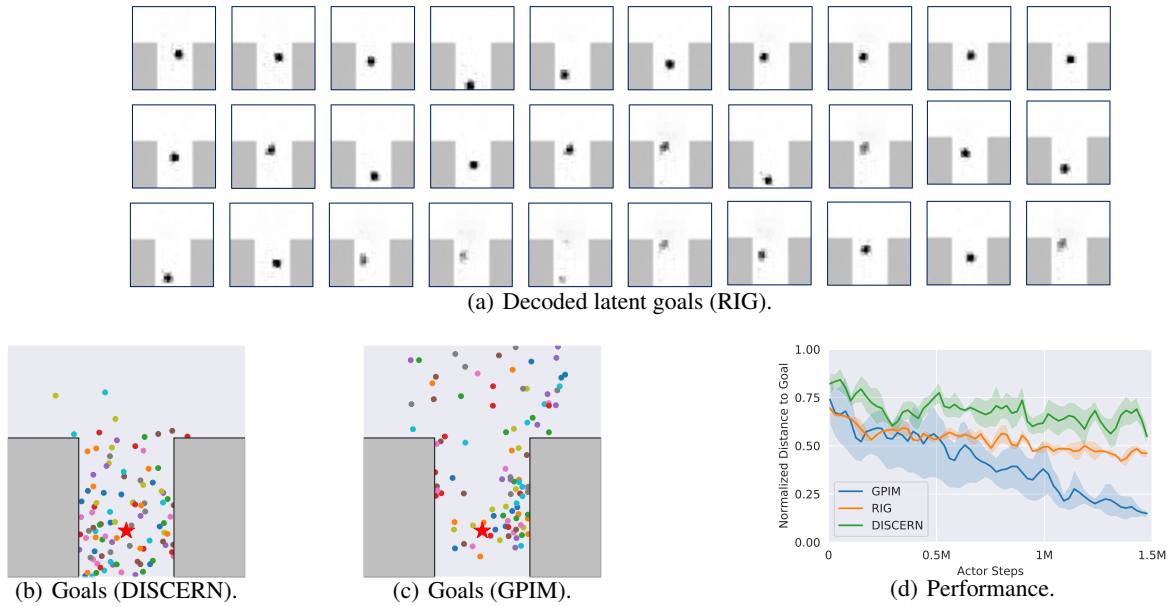


Figure 14: Distribution of sampled goals for the goal-conditioned policy, where the initial state is $[5,2]$ (the red star) and the actor step is 20 for each rollout. (a) The goals (images) are obtained by decoding 30 sampled latent goals z_g in VAE framework; (b) The goals (colored dots) are sampled from the agent’s behaviors by random exploration; (c) The goals (colored dots) are relabeled from the states induced by our latent-conditioned policy. (d): Evaluation on reaching user-specified goals, where GPIM significantly outperforms baselines.

goal space. The decoded latent goals are shown in Figure 14(a), where we sample 30 goals. It is shown that the majority of goals are also between the two obstacles because the goals for training the VAE prior come from the same distribution as in DISCERN.

Our method, GPIM, obtains goals from the behaviors induced by the latent-conditioned policy. Maximizing $\mathcal{I}(s; \omega)$ encourages different skills to induce different states that are further relabeled to goals. This objective ensures that each skill individually is distinct and the skills collectively explore large parts of the state space (Eysenbach et al. 2018). As shown in Figure 14(c), our method provides better coverage of the state space than DISCERN and RIG.

Figure 14(d) shows the performance of the three methods, where we randomly sample goals from the whole state (or goal) space at test phase. We can see that our method significantly outperforms the baselines. The most common failure mode for prior methods is that the goal distribution collapses (Pong et al. 2019), causing that the agent can reach only a fraction of the state space, as shown in Figure 14(a) and 14(b).

Exploration is a well-studied problem in the field of RL, and there are many proven approaches with different benefits to improve the exploration (Campos et al. 2020; Colas, Sigaud, and Oudeyer 2018; Pitis et al. 2020). Note that these benefits are orthogonal to those provided by our straightforward GPIM, and these approaches could be combined with GPIM for even greater effect. We leave combing our method with sophisticated exploration strategies to future work.

7.5 Training with Underspecified Latent (Support) Space

Here we show that underspecified latent (support) space may induce a large performance gap for learning the goal-conditioned policy. Qualitatively, Theorem 1 explains the performance gap induced by $p(s|\omega, \mu^*)$ and highlights that such gap is sensitive to the prior latent distribution $p(\omega)$. We thus add additional experiments on the distribution of skills on 2D Navigation, Object manipulation and Fetch tasks, as shown in Table 1.

Table 1: 2D Nav.: taks 2D navigation; task object manipulation.

	Discrete; 5 skills	Discrete; 10 skills	Discrete; 50 skills	Discrete; 100 skills	Continuous
2D Nav.	0.296 (+/- 0.091)	0.152(+/- 0.066)	0.137 (+/- 0.052)	0.132 (+/- 0.037)	0.122 (+/- 0.044)
O-M	0.535 (+/- 0.110)	0.321 (+/- 0.082)	0.199 (+/- 0.057)	0.193 (+/- 0.064)	0.182 (+/- 0.060)
Fetch	0.376 (+/- 0.175)	0.320 (+/- 0.104)	0.257 (+/- 0.089)	0.162 (+/- 0.057)	0.149 (+/- 0.033)

We found that the number of skills does affect the performance of the goal-conditioned policy. In simple tasks (2D navigation task), the effect is relatively small. But in complex environments, this effect cannot be ignored. We analyze the generated goal distributions in these experiments with different numbers of skills and found that goals generated by a small number of skills are extremely sparse, leading to the bias of the goal-conditioned policy. Nevertheless, such bias can be reduced, to some extent. As shown in 2D navigation task, learning with 10 skills can still produce comparable results. We attribute this result to the policy’s generalization ability and the perception-level loss (Appendix 7.3).

7.6 Training with Unfixed Initial State

In Assumption (the main text), we assume that the initial state of the environment is fixed. For granting valid training for each rollout of the goal-conditioned π_θ , we need to keep the initial state fixed or filter out initial states (for goal-conditioned π_θ , see Line 14 in Algorithm 1) that never lead to the relabeled goals, eg. constraining $\text{Distance}(\tilde{s}_0, s_0) \leq \epsilon$.

However, although randomly sampling initial states for π_μ and π_θ from the initial distribution (more than one fixed state) can not guarantee that the coming training (for π_θ) must be valid (goals are reachable), a large number of samples will ensure that there exist cases where initial states obtained by two consecutive resets is close, which can enable valid training. We also validate such setting (more than one fixed initial state) in 2D navigation (x-y goal) and 2D navigation (color-shape goal) tasks, as shown in Figure 15. We can observe that 1) such performance is reduced compared to the fixed starting point setting, and 2) the performance of our method outperforms that of DISCERN with the same initial state distribution (more than one fixed state).

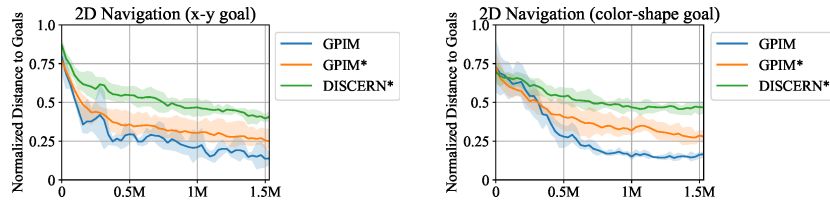


Figure 15: GPIM: training GPIM with the fixed initial state $[0,0]$. GPIM*: training GPIM with the initial state distribution (uniformly sampled from $[0,0]$, $[-0.25, -0.25]$, $[-0.25, 0.25]$, $[0.25, -0.25]$, $[0.25, 0.25]$). DISCERN*: training DISCERN with the initial state distribution (uniformly sampled from $[0,0]$, $[-0.25, -0.25]$, $[-0.25, 0.25]$, $[0.25, -0.25]$, $[0.25, 0.25]$).

7.7 The Robustness of GPIM on Stochastic MDP

Here we show the robustness of our GPIM on stochastic MDP. We add random noise to the dynamics of the environment 2D navigation, so as to build the stochastic MDP: $p(s'|s, \pi(s)) \rightarrow p(s'|s, \pi(s) + \text{action-space.sample}(\cdot) \cdot \Delta)$, where we sample a random action from the action space and then weigh the action and the action output from the policy with Δ . Thus, we can use Δ to represent the stochasticity of the environment.

We show our results in the stochastic environments in Figure 16. We can find that when equals 0.1, the learning process is hardly affected. As the stochasticity of the environment increases, the performance of the method decreases. When Δ equals 0.5, the method barely completes the task.

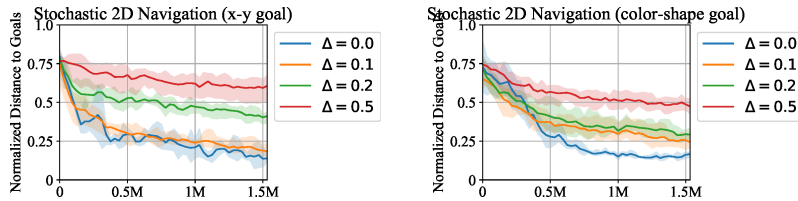


Figure 16: Evaluation on the stochastic MDP.

8 Derivation

8.1 Derivation of the Variational Bound

$$\begin{aligned}
& \mathbb{E}_{p_m(\cdot)} [\log p(\omega|s) + \log p(\omega|\tilde{s}) - 2 \log p(\omega)] \\
&= \mathbb{E}_{p_m(\cdot)} [\log q_\phi(\omega|s) + \log q_\phi(\omega|\tilde{s}) - 2 \log p(\omega)] \\
&\quad + \underbrace{\mathbb{E}_{p_m(\cdot)} [KL(p(\omega|s)||q_\phi(\omega|s)) + KL(p(\omega|\tilde{s})||q_\phi(\omega|\tilde{s}))]}_{\geq 0} \\
&\geq \mathbb{E}_{p_m(\cdot)} [\log q_\phi(\omega|s) + \log q_\phi(\omega|\tilde{s}) - 2 \log p(\omega)]
\end{aligned}$$

8.2 Proof of Theoretical Guarantees

Note that

$$\eta(\pi_\theta) = \mathbb{E}_{p'(g, \tilde{s}; \theta)} [\log p'(g|\tilde{s}) - \log p'(g)],$$

and

$$\hat{\eta}(\pi_\theta) = \mathbb{E}_{p(\omega, s, g, \tilde{s}; \mu^*, \kappa, \theta)} [\log p(\omega|\tilde{s}) - \log p(\omega)],$$

where $\mu^* = \arg \max_\mu \mathcal{I}(s; \omega)$. For deterministic π_μ , we have $\mathbb{E}_{p(\omega, s; \mu^*)} \log p(s|\omega; \mu^*) = 0$.

Thus, we have:

$$\begin{aligned} & \hat{\eta}(\pi_\theta) - \eta(\pi_\theta) && \# p_m^*(\cdot) \triangleq p(\omega, s, g, \tilde{s}; \mu^*, \kappa, \theta) \\ &= \mathbb{E}_{p_m^*(\cdot)} [\log p(\omega|\tilde{s}) - \log p(\omega)] - \mathbb{E}_{p'(g, \tilde{s}; \theta)} [\log p'(g|\tilde{s}) - \log p'(g)] \\ &= \underbrace{\mathbb{E}_{p_m^*(\cdot)} [\log p(\omega|\tilde{s}) - \log p(\omega) - \log p'(g|\tilde{s}) + \log p'(g)]}_{\text{TERM-I}} \\ &+ \underbrace{\mathbb{E}_{p_m^*(\cdot)} [\log p'(g|\tilde{s}) - \log p'(g)] - \mathbb{E}_{p'(g, \tilde{s}; \theta)} [\log p'(g|\tilde{s}) - \log p'(g)]}_{\text{TERM-II}}. \end{aligned}$$

Special case: If we assume the prior goal distribution $p'(g)$ for optimizing $\eta(\pi_\theta)$ matches the goal distribution $p(g|\omega; \mu^*, \kappa)$ induced by π_{μ^*} and f_κ for optimizing $\hat{\eta}(\pi_\theta)$, e.g., $\mathbb{E}_\omega [p(g|\omega; \mu^*, \kappa)] = p'(g)$, thus we have $p_m^*(\cdot) \triangleq p(\omega, s; \mu^*)p(g, \tilde{s}|s; \kappa, \theta) = p(\omega, s; \mu^*)p'(g, \tilde{s}; \theta)$. By inserting this equation into $\hat{\eta}(\pi_\theta) - \eta(\pi_\theta)$, we obtain

$$\text{TERM-II} = 0,$$

and

$$\begin{aligned} \text{TERM-I} &= \mathbb{E}_{p_m^*(\cdot)} [\log p(\omega|\tilde{s}) - \log p(\omega) - \log p'(g|\tilde{s}) + \log p'(g)] \\ &= \mathbb{E}_{p_m^*(\cdot)} \left[\log \left(\frac{p(\omega, \tilde{s})}{p(\tilde{s})p(\omega)} \right) - \log \left(\frac{p'(g, \tilde{s})}{p'(\tilde{s})p'(g)} \right) \right] \\ &= \mathbb{E}_{p_m^*(\cdot)} \left[\log p(\tilde{s}|\omega) - \log p'(\tilde{s}|g) - \underbrace{\log p(\tilde{s}) + \log p'(g)}_{=0} \right] \\ &= \mathbb{E}_{p_m^*(\cdot)} [\log p(\tilde{s}|\omega; \mu^*, \kappa, \theta) - \log p(\tilde{s}|g; \theta)] \\ &= \mathbb{E}_{p_m^*(\cdot)} [\log p(s, g, \tilde{s}|\omega; \mu^*, \kappa, \theta) - \log p(\tilde{s}|g; \theta)] \quad \# \pi_{\mu^*} \text{ is deterministic} \\ &= \mathbb{E}_{p(\omega, s, g; \mu^*, \kappa)} [\log p(s|\omega; \mu^*) + \log p(g|s; \kappa)] \\ &= 0. \quad \# \pi_{\mu^*} \text{ is deterministic} \end{aligned}$$

General case: If $\mathbb{E}_\omega [p(g|\omega; \mu^*, \kappa)] \neq p'(g)$, e.g., $p_m^*(\cdot) \triangleq p(\omega, s; \mu^*)p(g, \tilde{s}|s; \kappa, \theta) \neq p(\omega, s; \mu^*)p'(g, \tilde{s}; \theta)$, we apply Holder's inequality and Pinsker's inequality over TERM-II. Then the following inequality holds:

$$\begin{aligned} \text{TERM-II} &= \mathbb{E}_{p(\omega, s; \mu^*)} [\mathbb{E}_{p(g, \tilde{s}|s; \kappa, \theta)} [R(g, \tilde{s})] - \mathbb{E}_{p'(g, \tilde{s}; \theta)} [R(g, \tilde{s})]] \\ &\leq \mathbb{E}_{p(\omega, s; \mu^*)} [\|R(g, \tilde{s})\|_\infty \cdot \|p(g, \tilde{s}|s; \kappa, \theta) - p'(g, \tilde{s}; \theta)\|_1] \\ &\leq \mathbb{E}_{p(\omega, s; \mu^*)} \left[\left(\max_{g, \tilde{s}} R(g, \tilde{s}) \right) \cdot 2\sqrt{\frac{1}{2} D_{\text{KL}}(p(g, \tilde{s}|s; \kappa, \theta) \| p'(g, \tilde{s}; \theta))} \right] \\ &= \mathbb{E}_{p(\omega, s; \mu^*)} \left[\left(\max_{g, \tilde{s}} R(g, \tilde{s}) \right) \cdot 2\sqrt{\frac{1}{2} D_{\text{KL}}(p(g|s; \kappa) \| p'(g))} \right], \end{aligned}$$

where $R(g, \tilde{s}) = \log p'(g|\tilde{s}) - \log p'(g)$.

Assuming the goal space is the same as the state space and relabeling f_κ is bijective, we can ignore the relabeling term $p(g|s; \kappa)$ and replace $p'(g)$ with $p'(s)$. Thus, we have

$$\text{TERM-II} \leq \left(\max_{g, \tilde{s}} R(g, \tilde{s}) \right) \cdot \mathbb{E}_{p(\omega)} \left[2\sqrt{\frac{1}{2} D_{\text{KL}}(p(s|\omega; \mu^*) \| p'(s))} \right].$$

9 Implementation Details

9.1 Relabeling over the Environment

Applying our GPIM on 2D navigation (*color-shape goal*) may cause that the color and shape of the goal that relabeled from a state that does not represent a valid goal in the reset environment (since valid goals are only ones that can be reached by the agent reach *after* this reset). In Algorithm 1 (in the main text), the goals are claimed to be generated by π_μ while there may be no corresponding target in the reset environment for training π_θ . Thus, at the step that we reset the environment for training π_θ (line 14), we make this reset is associated with the generated goal by π_μ and f_κ . See Algorithm 2 for the details.

Algorithm 2: Learning process of our proposed GPIM (with relabeling over the environment)

```
1: while not converged do
2:   # Step I: generate goals and reward functions.
3:   Sample the latent variable:  $\omega \sim p(\omega)$ .
4:   Reset Env. & sample initial state:  $s_0 \sim p_0(s)$ .
5:   for  $t = 0, 1, \dots, T - 1$  steps do
6:     Sample action:  $a_t \sim \pi_\mu(a_t|s_t, \omega)$ .
7:     Step environment:  $s_{t+1} \sim p(s_{t+1}|s_t, a_t)$ .
8:     Relabel:  $g_t = f_\kappa(s_{t+1})$ .  $\triangleright$  Record.
9:     Compute reward  $r_t$  for policy  $\pi_\mu$  using (5).
10:    Update policy  $\pi_\mu$  to maximize  $r_t$  with SAC.
11:    Update discriminator ( $q_\phi$ ) to maximize  $\log q_\phi(\omega|s_{t+1})$ 
    with SGD.
12:   end for
13:   # Step II:  $\pi_\theta$  imitates  $\pi_\mu$  with the relabeled goals and the as-
    sociated rewards (for the same  $\omega$ ). Here we only consider
    the static goal for  $\pi_\theta$ .
14:   Reset Env. with the relabeled goals  $g_T$  & sample initial
    state:  $\tilde{s}_0 \sim p_0(\tilde{s})$ .
15:   for  $t = 0, 1, \dots, T - 1$  steps do
16:      $g_t = g_T$  for fixed (static) goals.
17:     Sample action:  $a_t \sim \pi_\theta(a_t|\tilde{s}_t, g_t)$ .
18:     Step environment:  $\tilde{s}_{t+1} \sim p(\tilde{s}_{t+1}|\tilde{s}_t, a_t)$ .
19:     Compute reward  $\tilde{r}_t$  for policy  $\pi_\theta$  using (8).
20:     Update policy  $\pi_\theta$  to maximize  $\tilde{r}_t$  with SAC.
21:   end for
22: end while
```

9.2 Environment Details

We introduce the details of environments and tasks here, including the environment setting of 2D navigation (*x-y goal* and *color-shape goal*), object manipulation, three atari games (seaquest, berzerk and montezuma revenge), and the mujoco tasks (swimmer, half cheetah and fetch).

2D navigation tasks: In 2D navigation tasks, the agent moves in each of the four cardinal directions, where the states denote the 2D location of the agent. We consider the following two tasks: moving the agent to a specific coordinate named *x-y goal* and moving the agent to a specific object with certain color and shape named *color-shape goal*.

- **2D Navigation (*x-y goal*):** The size of the environment is 10×10 (continuous state space) or 7×7 (discrete state space). The state is the location of the agent, and the goal is the location of the final location.
- **2D Navigation (*color-shape goal*):** The size of the environment is 10×10 . The state consists of the locations of the agent and three objects with different color-shape pairs (one real target and two distractors). The goal is described by the color and shape of the real target, encoded with one-hot.

Object manipulation: More complex manipulation considers a moving agent in 2D environment with one block for manipulation, and the other as a distractor. The agent first needs to reach the block and then move the block to the given location, where the block is described using color and shape. The size of the environment is 10×10 . The state consists of the locations of the agent and two blocks with different color-shape pairs (one real target and one distractor). The goal consists of the one-hot encoding of the color-shape of the target block that needs to be moved, and the 2D coordinate of the final location of the movement.

Table 2: The repetition length of the action.

Environments	k
Seaquest-ram-v0	2, 3, 4, 5
Berzerk-ram-v0	34, 36, 38, 40
MontezumaRevenge-ram-v0	2, 3, 4, 5

Atari games: We test the performance on three atari games: seaquest, berzerk, and montezuma revenge. In order to reduce the difficulty of training, we adopt the RAM-environment (i.e., Seaquest-ram-v0, Berzerk-ram-v0, and MontezumaRevenge-ram-v0), where each state represents a 128-dimensional vector. Each action repeatedly performs for a duration of k frames, where k is uniformly sampled from Table 2.

Mujoco tasks: We consider to make diverse agents to fast imitate a given goal trajectory, including the imitation of behaviors of a swimmer, a half cheetah, and a fetch, where states in the trajectory denote positions of agents. Such experiments are conducted to demonstrate the effectiveness of our proposed method in learning behaviors over a continuous high-dimensional action space, which is more complicated in physics than the 2D map.

Note that the goals in all the experiments are images $50 \times 50 \times 3$ (3 channels, RGB) in size, except that the *color-shape goal* is encoded with one-hot.

9.3 Tracking Hand Movement

For the dynamic (time-varying) goals, we implement the hand movement tracking with MediaPipe (Lugaresi et al. 2019) to extracting features of hand from images. As shown in Figure 17, we adopt two cameras to get the up-view and the left-view of hand, respectively. Then the two views are processed by MediaPipe to locate the hand, which allows us to get the position in three dimensions. Finally, we make the panda robot track the extracted 3D coordinate with the trained goal-conditioned policy π_θ .



Figure 17: We adopt two cameras to locate the hand for the movement tracking task.

9.4 Metrics, Network Architectures and Hyperparameters

Here we give a clear definition of our evaluation metric – ”normalized distance to goal”:

I: When the goal is to reach the final state of the trajectory induced by π_μ , the distance to goal is the L2-distance between the final state \tilde{s}_T^k induced by $\pi_\theta(\cdot|\cdot, g^k)$ and the goal state g^k randomly sampled from the goal (task) space:

$$Dis = \frac{1}{N} \sum_{k=1}^N L2(\tilde{s}_T^k, g^k),$$

where N is the number of testing samples. We set $N = 50$ for 2D navigation, object manipulation and atari games (seaquest, berzerk and montezuma revenge).

II: When the goal is to imitate the whole trajectory induced by π_μ , the distance is the expectation of distance over the whole trajectory $\{\tilde{s}_0^k, \tilde{s}_1^k, \dots, \tilde{s}_T^k\}$ induced by $\pi_\theta(\cdot|\cdot, g_t^k)$ and goal trajectory $\{g_0^k, g_1^k, \dots, g_{T-1}^k\}$ randomly sampled from the trajectory (task) space:

$$Dis = \frac{1}{N} \sum_{k=1}^N \left(\frac{1}{T} \sum_{t=1}^T L2(\tilde{s}_t^k, g_{t-1}^k) \right),$$

where N is the number of testing samples. We set $N = 50$ for mujoco tasks (swimmer, half cheetah and fetch) .

The term ”normalized” means that the distance is divided by a scale factor.

Note that, for three atari games (seaquest, berzerk, and montezuma revenge), the L2-distance for evaluation³ is the difference between the position of controllable agent and the target’s position, where the position is obtained by matching the pixel on the imaged state.

In our implementation, we use two independent SAC architectures (Haarnoja et al. 2018) for latent-conditioned policy π_μ and goal-conditioned policy π_θ . We find empirically that having two networks share a portion of the network structure will degrade the experimental performance. We adopt universal value function approximates (UVFAs) (Schaul et al. 2015) for extra input (goals). For the latent-conditioned policy π_μ , to pass latent variable ω to the Q function, value function and policy, as in DIAYN, we simply concatenate ω with the current state s_t (and action a_t). For goal-conditioned policy π_θ , we also concatenate g_t with current state \tilde{s}_t (and action a_t). We update the ϑ_E using the gradients from both the *Dis_Loss* and Q function’s loss of the goal-conditioned policy π_θ .

The latent-distributions are provided in Table 3 and the hyper-parameters are presented in Table 4.

10 More Results

10.1 Comparison on the Atari tasks

In Figure 18, we provide more results on the Atari tasks.

³The reward function for our baseline **L2 Distance** still calculates the L2-distance directly on the original state space, instead of the distance of the agents’ positions after pixel matching here.

Table 3: The given latent distribution for each tasks in our experiments.

Arrow Discrete; 3 skills	2D navigation Continuous; $[-1, 1]^2$	Object manipulation Continuous; $[-1, 1]^2$	Atari games Continuous; $[-1, 1]^2$
Half-cheetah Discrete; 50 skills	Fetch; Panda Continuous; $[-1, 1]^3$	Maze (Figure 8) Discrete; 10 skills	2D navigation (Appendix 1.4) Discrete; 10 skills
Swimmer Discrete; 50 skills	Gridworld Discrete; 4 skills		

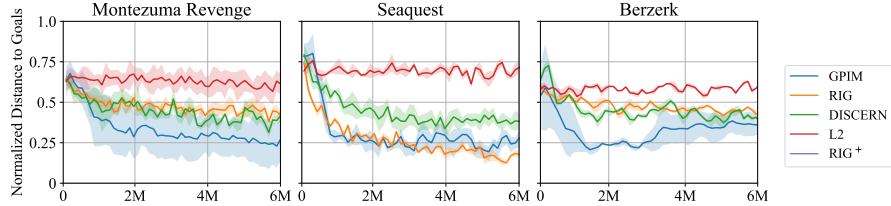


Figure 18: Performance (normalized distance to goals vs. actor steps) of our GPIM and baselines.

10.2 Learned Behaviors on temporally-extended tasks

More experimental results are given in Figure 19 to show the imitation on several temporally-extended tasks.

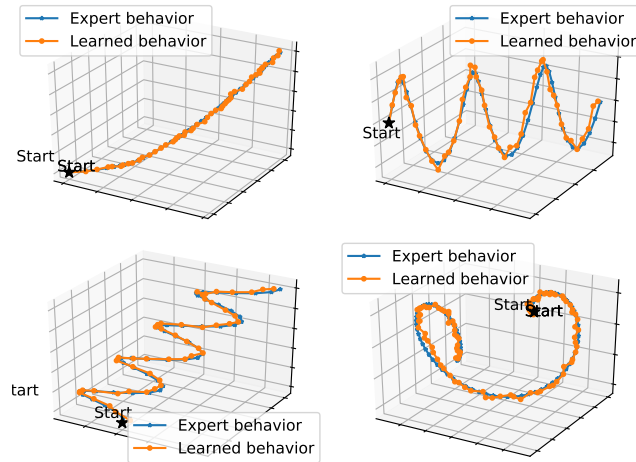


Figure 19: Expert behaviors and learned behaviors. The four expert trajectories are described parametrically as: $(x, y, z) = (\log_{10}(t+1) + t/50, \sin(t)/5 + t/5, t/5)$, $(x, y, z) = (t/5, \cos(t)/5 - 1/5 + t/5, \sin(t)/5)$, $(x, y, z) = (\cos(t)/5 + t/50 - 1/1, \sin(t)/5 + t/5, t/5)$, and $(x, y, z) = (\sin(t) - \sin(2t)/2, -t/5, \cos(t)/2 - \cos(2t)/2)$.

10.3 Learned Behaviors from GPIM

More experimental results are given in Figure 20 to show the learned behaviors on 2D navigation, object manipulation, three atari games (seaquest, berzerk and montezuma revenge), and the mujoco tasks (swimmer, half cheetah and fetch). Videos are available under <https://sites.google.com/view/gpim>.

Broader Impact

The main concern in the research area of unsupervised RL is how to find numerous diverse goals as well as associated reward functions. Particularly, in practical application, the goal and state are often heterogeneous data with high variability of data types and formats, which further aggravates the difficulty of reward learning. Our model addresses these problems by introducing a latent-conditioned policy and the relabeling procedure, scoring current states with latent variables, instead of goals. Although the manifold spaces of goals and latent variables are inconsistent, we show that this relabeling procedure can still effectively learn policy.

However, by autonomous exploration of the environment, the agent is likely to generate some useful behaviors as well as the majority of useless skills. Of particular concern is that the use of autonomous exploration is likely to generate a strategy that will induce dire consequences, such as a collision skill in an autonomous driving environment. How to generate useful behaviors for user-specified tasks and how to use these induced skills are also open problems. An alternative solution is to use an extrinsic reward or the offline data (IRL, offline RL) to guide the exploration. While another issue comes from the exploration-exploitation trade-off. We would encourage further work to understand the limitations of GPIM interacting with the environment autonomously. We would also encourage research to understand the risks arising from autonomous robot learning.

Another limitation is that our learning framework needs an extra latent-conditioned policy training for relabeling goals and providing a reward function. This may require twice as much interaction time with the environment as learning a single policy network. For practical application, a simulation platform is preferred for such expensive training. Thus, one promising direction is to mitigate the difference between the simulation platform and the actual environment. We also encourage researchers to pursue the effective methods for transfer learning.

Table 4: Hyper-parameters

Hyper-parameter		value	
Batch Size		256	
Discount Factor		0.99	
Buffer Size		10000	
Smooth coefficient		0.05	
Temperature		0.2	
Learning Rate	2D Navigation	x-y goal	0.001
		color-shape goal	0.001
	Object Manipulation		0.001
	Mujoco tasks	Swimmer	0.0001
		HalfCheetah	0.0001
		Fetch	0.0001
	Atari games	Seaquest	0.0003
		Berzerk	0.0003
		Montezuma Revenge	0.0003
	Path Length	2D Navigation	x-y goal
color-shape goal			20
Object Manipulation		20	
Mujoco tasks		Swimmer	50
		HalfCheetah	50
		Fetch	100
Atari games		Seaquest	25
		Berzerk	25
		Montezuma Revenge	25
Hidden Size		2D Navigation	x-y goal
	color-shape goal		128
	Object Manipulation		128
	Mujoco tasks	Swimmer	256
		HalfCheetah	256
		Fetch	256
	Atari games	Seaquest	256
		Berzerk	256
		Montezuma Revenge	256
	Dimension of Generative Factor	2D Navigation	x-y goal
color-shape goal			2
Object Manipulation		4	
Mujoco tasks		Swimmer	3
		HalfCheetah	4
		Fetch	4
Atari games		Seaquest	16
		Berzerk	16
		Montezuma Revenge	16
α		1	
γ		5	
δ_{pixel}		255	

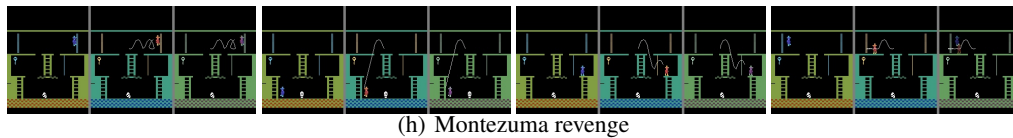
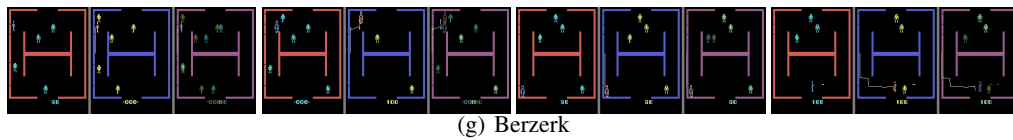
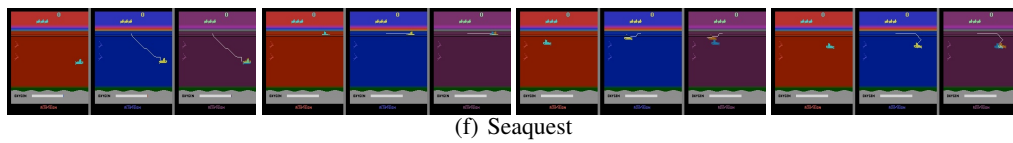
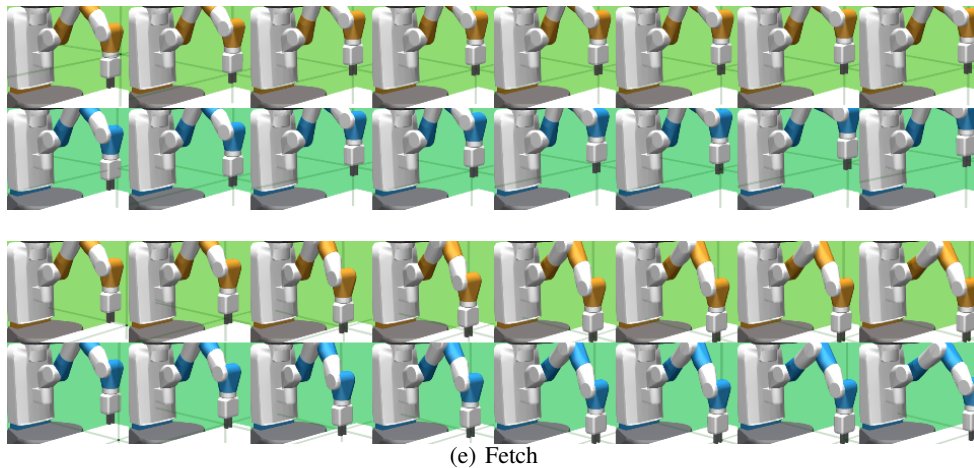
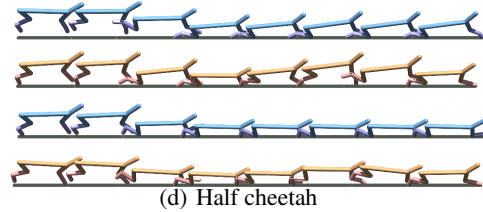
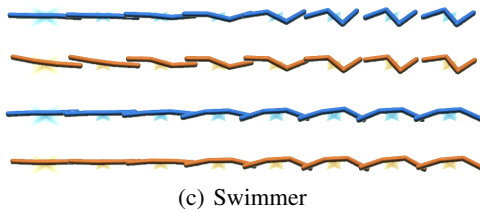
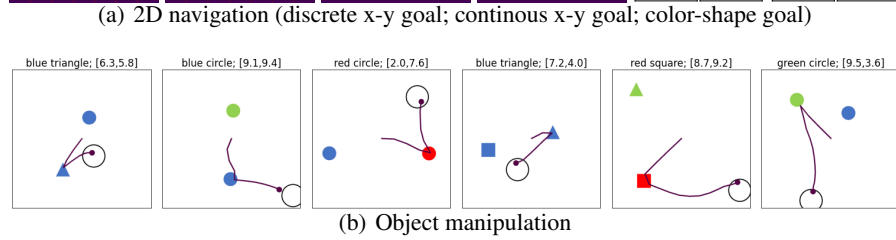
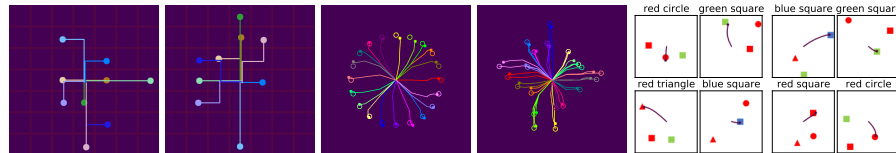


Figure 20: Discovered goal-conditioned behaviors. (f-h): The left subfigure shows the expert behaviors (goals); The middle subfigure shows the learned behaviors by GPIM; The right subfigure is the stacked view of goals and GPIM behaviors.